Title: A high-throughput screen identifies RNA binding proteins that affect fertility in *Caenorhabditis elegans* and reveals a functional relationship between ADR-2 and SQD-1

Emily A. Erdmann[1], Melanie Forbes[2], Margaret Becker[3], Sarina Perez[2], Mary Skelly[2], Heather A. Hundley[2#]

1. Genome, Cell and Developmental Biology Graduate Program, Indiana University, Bloomington IN, US 47405
2. Department of Biology, Indiana University, Bloomington IN, US 47405
3. Medical Sciences Program, Indiana University School of Medicine-Bloomington, Bloomington IN, US 47405

#Corresponding author: hahundle@indiana.edu

Running Title: RBP fertility screen reveals ADR-2/SQD-1 interaction

ABSTRACT

RNA binding proteins play essential roles in coordinating germline gene expression and development in all organisms. Characterization of gross fertility defects, such as sterility, has identified RNA binding proteins that are critical regulators of germline gene expression; however, broader screens for RNA binding proteins involved in specific reproductive processes are lacking. Here, a reverse genetic screen was performed to identify RNA binding proteins that impact yolk and embryo production in *Caenorhabditis elegans* hermaphrodites. This screen makes use of animals expressing a vitellogenin (yolk protein) fusion with green fluorescent protein, in a genetic background that corrects for a previously identified fertility defect in this strain. From this screen, we identified 23 RNA binding proteins that regulate embryo production in *Caenorhabditis elegans*. This screen lays groundwork for future interrogations into the molecular roles of these proteins in yolk production and embryogenesis. Additionally, the screen uncovered a genetic interaction between ADR-2, a member of the Adenosine DeAminase Acting on RNA (ADAR) family, and SQD-1, a member of the heterogenous nuclear ribonucleoprotein (hnRNP) family. Transcriptome-wide assessment in animals depleted of *sqd-1* revealed over 8000 misregulated transcripts, suggesting SQD-1 is a major regulator of gene expression. Consistent with this, microscopy and reproductive assays reveal that *sqd-1* is essential for oogenesis. In the absence of *adr-2*, the effects of loss of *sqd-1* on gene expression are attenuated, as well as the defects in oogenesis. Together, these data indicate that both ADR-2 and SQD-1 are important regulators of germline gene expression and oogenesis.

Article Summary

The molecular information that controls early development is RNA. Interactions between RNA and RNA binding proteins are critical for successful reproduction across species. In this study,

over 250 RNA binding proteins were assessed for effects on yolk and embryo production in *Caenorhabditis elegans*. Twenty-three regulators of these important reproductive steps were identified, including 7 novel regulators. This screen also revealed a genetic interaction between two RNA binding proteins, SQD-1 and ADR-2, which impacts germline gene expression, oogenesis, and fertility.

Keywords: ADAR, hnRNP, post-transcriptional gene regulation, germline, vitellogenesis, yolk, reproduction, oogenesis, RNA binding protein (RBP)

Introduction

Underlying successful reproduction is a complex gene regulatory network that coordinates many cellular and molecular events to ensure proper reproductive timing, development of gametes, and embryogenesis. Because many of these processes require rapid responses to signals or transient gene expression changes during times of transcriptional quiescence, RNA-level regulation is highly relied upon in germ cells and supporting tissues to coordinate gene expression (Seydoux and Braun 2006). As such, many RNA binding proteins (RBPs) have been found to be highly expressed during gametogenesis and essential for reproduction (Albarqi and Ryder 2022; Nguyen-Chi and Morello 2011; Rosario and others 2017).

Caenorhabditis elegans is a useful model organism for germline studies because these animals exist mainly as hermaphrodites, producing both sperm and oocytes at different life stages. Studies of the *C. elegans* germline have identified RBPs that regulate stability and translation of specific transcripts to coordinate various reproductive processes, including germline stem cell renewal (Subramaniam and Seydoux 2003; Wang and others 2020), the transition from spermatogenesis to oogenesis (Bachorik and Kimble 2005; Datla and others 2014; Kim and others 2012; Yoon and others 2017; Zanetti and others 2012) and from mitosis to meiosis (Kimble and Crittenden 2007; Park and others 2020; Priti and Subramaniam 2015) as well as proper progression through meiosis (Albarqi and Ryder 2022; Spike and others 2014).

Prior to fertilization, yolk provisioning is one of the final steps in *C. elegans* oogenesis and is also known to be regulated by at least one RBP (Lee and Schedl 2001). While viable embryos can be formed in the absence of yolk (Van Rompay and others 2015), yolk contributes to the fitness of progeny (Dowen and Ahmed 2019; Jordan and others 2019; Kern and others 2021). As such, *C. elegans* invest an enormous amount of resources into yolk production during adulthood, even sacrificing their own bodily integrity toward the goal of producing sufficient yolk for their progeny (Ezcurra and others 2018; Gems and others 2021; Sornda and others 2019). A major component of yolk is vitellogenin, or yolk protein. Vitellogenins are synthesized in the adult intestine, then exported into the body cavity and taken up into developing oocytes via receptor-mediated endocytosis (Kimble and Sharrock 1983). The *C. elegans* yolk receptor, RME-2, was discovered in a study using a transgenic fusion of the vitellogenin gene *vit-2* and green fluorescent protein (*gfp*) to visualize yolk endocytosis (Grant and Hirsh 1999). Since that publication, the transgenic *vit-2::gfp* strain has been used in a variety of studies as a reporter for vitellogenesis, receptor-mediated endocytosis, and fertility more generally (Balklava and others

2007; Balklava and others 2016; Seah and others 2016; Van Rompay and others 2015). In a previous study, we found that the *vit-2::gfp* strain contains fewer embryos and produces fewer progeny than wild-type animals (Erdmann and others 2022).

Here, we describe our finding that the fertility defects of *vit-2::gfp* animals are rescued in animals lacking *adr-2*, a member of the Adenosine DeAminase acting on RNA (ADAR) family of RNA binding proteins. ADARs bind double-stranded RNA and can affect gene expression either through binding transcripts or by catalyzing the deamination of adenosine (A) to inosine (I), known as A-to-I RNA editing (Erdmann and others 2021; Goldeck and others 2022; Savva and others 2012). ADR-2 is the sole A-to-I RNA editing enzyme in *C. elegans* (Arribere and others 2020), and has been shown to play important roles in chemotaxis (Deffit and others 2017; Tonkin and others 2002) as well as resistance to pathogen infection (Dhakal and others 2023) and hypoxia (Mahapatra and others 2023).

Using *adr-2(-);vit-2::gfp* animals as a defect-adjusted background, we performed a high-throughput reverse genetic screen to identify RBPs that affect fertility. As mentioned previously, roles for several RBPs in the *C. elegans* germline have been identified; however, epistatic and compensatory interactions may have obscured the identification of other important factors in RNA regulation in germ cells and supporting cells. In addition to identifying several high-confidence regulators of fertility, the screen revealed a genetic interaction between *adr-2* and *sqd-1*, an RNA binding protein orthologous to *Drosophila melanogaster* Squid and *Homo sapiens* hnRNPs (heterogeneous nuclear ribonucleoproteins) (Kim and others 2018; Shaye and Greenwald 2011). While *sqd-1* has not been well-characterized in *C. elegans*, a genome-wide RNA interference (RNAi) screen previously reported that decreased *sqd-1* expression impacted fertility in *C. elegans* (Maeda and others 2001). SQD-1 has also been reported to physically interact with GLD-1 (Akay and others 2013), an RBP known to regulate RNA patterning and translational repression in the germline (Scheckel and others 2012). The *Drosophila* homolog of *sqd-1*, *squid*, is known to direct embryo patterning via RNA localization (Clouse and others 2008; Goodrich and others 2004; Kelley 1993; Lall and others 1999; Norvell and others 1999) and has recently been shown to be required for germline stem cell maintenance (Finger and others 2023).

Here, we report the first unbiased characterization of gene expression changes in animals lacking *sqd-1* and observe thousands of transcripts are misregulated upon depletion of *sqd-1*. Additionally, we present evidence that *sqd-1* and *adr-2* extensively coregulate transcripts important for fertility. These data suggest a functional relationship between SQD-1 and ADR-2 and provide the first evidence that ADR-2 plays a role in germline gene regulation. Finally, we report the effects of depleting *sqd-1* on the morphology of the oogenic germline and show that loss of *adr-2* restores proper germline morphology to animals lacking *sqd-1*.

Materials and Methods

Worm strains and maintenance

All worm strains were maintained at 20ºC on nematode growth media (NGM) seeded with *Escherichia coli* OP50. Worms were thawed regularly from frozen stocks to minimize effects of accumulated random mutations. The following previously generated strains were used in this

study: Bristol Strain N2, BB20 (*adr-2(ok735)*) (Hundley and others 2008), HAH20 (*pwIs23[vit-2::gfp]*) (Erdmann and others 2022), *adr-2(uu28)* (a kind gift from Brenda Bass), HAH58 (3XFLAG::ADR-2) (Dhakal and others 2023).

Strains generated in this study include: HAH51 (*adr-2(ok735);pwIs[vit-2::gfp]*), HAH52 (*pwIs23[vit-2::gfp]*), HAH53 (*adr-2(uu28);pwIs23[vit-2::gfp]*), HAH55 (V5::SQD-1), HAH56 (V5::SQD-1; 3xFLAG::ADR-2). The V5::SQD-1 strain was made using standard microinjection techniques and *dpy-10* co-CRISPR to segregate successful CRISPR via rolling F1 progeny and non-rolling F2 progeny (Ghanta and others 2021). Injection mix for the V5::SQD-1 strain (HAH55) included 1.5 µM Cas9 (IDT, Alt-R Cas9 nuclease V3), 4 µM tracrRNA (IDT), 3µM of crRNA (IDT) (HH3122) (**Table S1**), 1 µM *dpy-10* crRNA (IDT) (HH3118) (**Table S1**), 0.25 µM *dpy-10* SSODN (HH2448) (**Table S1**), and 0.75µM of repair template ssODN (HH3158) (**Table S1**) containing the V5::SQD-1 sequence. Expression of V5::SQD-1 was confirmed by immunoblotting.

Crossed strains were made by placing 10-15 males and 1 hermaphrodite on mating plates (NGM plates seeded with a small spot of *E. coli* OP50 in the center) and genotyping was performed for the F1 progeny and F2 progeny using primers mentioned in **Table S1**. The specific crosses performed included: creation of HAH51 by crossing HAH20 hermaphrodites to BB20 males, creation of HAH52 and HAH53 by crossing HAH20 hermaphrodites to *adr-2(uu28)* males, creation of HAH56 by crossing HAH58 hermaphrodites to HAH55 males.

Brightfield and Fluorescence imaging

For **Figures 1A** and **3B**, imaged animals were mounted on 2% agarose pads in halocarbon oil and covered with a coverslip. Imaging was performed on a Zeiss SteREO Discovery V20. At least 10 animals were imaged per condition, representative images are shown in figures.
For **Figure 5**, germlines were extruded from animals grown on RNAi as described below. Germlines were fixed with 1% paraformaldehyde and methanol, permeabilized with 0.2% Triton X-100 (Sigma-Aldrich), and stained with DAPI (4′,6-diamidino-2-phenylindole) (Thermo Fisher Scientific). Germlines were mounted in Vectashield (VectorLabs) and imaged using a Leica SP8 Scanning Confocal microscope (Indiana University Light Microscopy Imaging Center). At least 10 germlines were imaged per condition, representative images shown in figures. Images were processed using ImageJ.

Embryo content assay

Performed as previously described (Erdmann and others 2022). Briefly, animals were synchronized by plating 20 gravid adults on each plate and allowing them to lay eggs for 3 hours before removing. Synchronized offspring were allowed to develop to day 1 adulthood. Twenty animals from each strain were placed in individual drops of 20% Arocep Ultra Bleach solution, and the cuticles were allowed to dissolve for ~10 minutes. The remaining embryos in each bleach drop were counted. The average embryo count from each set of 20 animals was calculated, representing one biological replicate. 3-5 biological replicates were performed for each strain.

Brood size assay

Performed as previously described (Erdmann and others 2022). Animals were synchronized as stated above. Two L4-stage animals of each strain were plated on each of 10 NGM plates seeded with *E. coli* OP50. The animals were moved to fresh plates each day for the remainder of the

experiment. Worms that died or crawled off the plate during the assay were excluded. Offspring laid on each plate were counted for two subsequent days after removal of the adults and divided by the number of adult animals plated on that plate, with adjustments made for animals that died or crawled off during the experiment. The experiment was ended when all adult animals produced no offspring for two consecutive days.

Bleaching

Synchronized animals were obtained by bleaching gravid adult animals with a solution of 5M NaOH (33%) and Sodium Hypochlorite (Fisher Scientific) (66%). After the solution was added, animals were incubated on a shaker at 20°C for 7 minutes and then spun down to collect embryos. Embryos were washed with 1X M9 buffer (22.0 mM KH_2PO_4, 42.3 mM Na_2HPO_4, 85.6 mM NaCl, 1 mM $MgSO_4$) solution thrice and incubated overnight in 1X M9 buffer at 20°C. The next day, hatched L1 worms were spun down and washed again with 1X M9 buffer thrice.

RNA interference

Animals were synchronized by bleaching and plated on RNAi plates (Plates with standard nematode growth medium, Ampicillin (50 µg/mL), Tetracycline (10 µg/mL), and IPTG (2mM)) seeded with HT115 bacteria containing RNAi vectors against various RNA binding proteins (RNAi vector collection a kind gift of Oliver Hobert, including plasmids compiled from the Ahringer and Vidal libraries) (**Table S2**). Each COPAS screening experiment also included animals fed with an empty RNAi vector and animals fed with an RNAi vector against GFP. After 3 days of growth at 20ºC, the animals on each plate were washed off with 1X M9 buffer.

GFP Quantification and data analysis

Synchronized young adult animals were run through the COPAS SELECT. The data were restricted to adult animals by eliminating all animals with time of flight values less than or equal to 120 or extinction values less than or equal to 176. The average GFP level for each sample was calculated, and values were normalized to the positive control (animals fed with an empty RNAi vector). RNAi vectors causing a >2.5 fold increase or decrease in GFP compared to the positive control were designated hits significantly affecting the phenotype. RNAi treatments that failed to produce young adult animals were excluded from screening.

Quantitative Real-Time PCR

RNA interference was performed as described above. Young adult animals were washed off RNAi plates with 1X M9 buffer, pelleted, and frozen in Trizol. RNA was extracted using standard Trizol-Chloroform extraction followed by treatment with TURBO DNase (Ambion) and cleanup with the RNeasy Extraction Kit (Qiagen). Reverse transcription was performed on total RNA using random hexamer primers, oligo dT, and Superscript III (Thermo Fisher). Gene expression was determined using KAPA SYBR FAST Master Mix (Roche) and gene-specific primers (**Table S1**) on a Thermo Fisher Quantstudio 3 instrument. The primers designed for qPCR spanned an exon-exon junction to prevent detection of genomic DNA in the samples. For each gene analyzed, a standard curve of 8 to 10 samples of 10-fold serial dilutions of the amplified product were used to generate a standard curve of cycle threshold versus the relative concentration of amplified product. Standard curves were plotted on a logarithmic scale in relation to concentration and fit with a linear line. Fit (r^2) values were around 0.99 and at least 7

data points fell within the standard curve. Each cDNA measurement was performed in 3 technical replicates, and each experiment was performed in 3 biological replicates.

RNA sequencing library preparation

RNAi and RNA extraction from young adult animals was performed as described above. Total RNA was subjected to Poly-A Selection using magnetic oligo(dT) beads (Invitrogen). Libraries were created from poly A-selected RNA using the KAPA RNA Hyperprep kit (Roche); cleanup steps were performed using AMPure XP beads (Beckman Coulter). Library fragment size distribution was determined via Tapestation electrophoresis (Agilent). Libraries were pooled by concentration and sequenced on two NextSeq 2000 P2 (100 cycle) flow cells (total 600 million single-end reads) at the Indiana University Center for Genomics and Bioinformatics.

Bioinformatic Analysis

Reads were aligned to a reference genome (*C. elegans* PRJNA13758 WS275) using STAR (version 2.7.10b). Differential gene expression analysis was performed in R with DESeq2 (Love and others 2014). Full code for these analyses is available at: https://github.com/emierdma/GSF3587/tree/main.

Co-Immunoprecipitation and immunoblotting

Mixed stage animals (strains HAH56 (V5::SQD-1; 3xFLAG::ADR-2) and N2) were washed from a well fed plate with 1X M9 buffer. After removing bacteria, the animals were resuspended in extract buffer (50 mM HEPES, pH 7.4; 70 mM K-Acetate, 5 mM Mg-Acetate, 0.05% NP-40 and 10% glycerol) containing 1 mini-Complete Protease inhibitor tablet (Roche) dissolved in 10 ml of buffer. The resulting mixture was dripped from a Pasteur pipet into liquid nitrogen, and pellets were stored at -80°C. Pellets were ground using a mortar and pestle on dry ice, then allowed to thaw at 4°C. Thawed lysates were centrifuged at 3220 rcf for 10 minutes to isolate the protein lysate. After determining the protein concentration using Bradford reagent (Sigma), a portion of the lysate was kept for immunoblotting (referred to as input) and 5 mg of lysate was added to 100 µl FLAG magnetic beads prepared in wash buffer with fresh detergents (0.5 M NaCl, 1X TBS, 0.1% NP-40, 0.25% Triton X-100) and 1 mini-Complete Protease inhibitor tablet. Each immunoprecipitation (IP) also contained 200 ul of wash buffer (0.5 M NaCl, 1X TBS), wherein 1 mini-Complete Protease inhibitor tablet was dissolved in 1 ml of wash buffer. After one hour on a nutator at 4°C, the magnetic beads were resuspended and washed three times in wash buffer with fresh detergents. After washing, the magnetic beads were resuspended in 2X SDS buffer (0.125 M Tris, 4% SDS, 10% glycerol, 0.02% bromophenol blue, 4% β-mercaptoethanol) and boiled for 5 minutes. Input and IP samples were subjected to SDS-PAGE and immunoblotted using either a FLAG (Sigma, MM8823) or V5 (Cell Signaling Tech, 13202S) antibody. SuperSignal West Pico PLUS Chemiluminescent Substrate (Fisher) and SuperSignal West Femto Maximum Sensitivity Substrate (Fisher) were used to visualize proteins via enhanced chemiluminescent detection. Images of the blots were taken on BIO-RAD ChemiDoc MP imaging system using Image Lab software (version 6.1.0 build 7).

Results

Loss of* adr-2 *rescues the fertility defect of* vit-2::gfp *worms

As previously reported, *C. elegans* expressing a transgenic fusion of the vitellogenin gene *vit-2* with *gfp* have a fertility defect resulting in fewer embryos in the uterus throughout reproductive

adulthood and an overall reduced brood size (Erdmann and others 2022). We noted that when the *vit-2::gfp* transgene was crossed into an *adr-2* deletion mutant (*adr-2(ok735)*) (Hundley and others 2008), the animals appeared similar in size and population density to wild-type animals lacking the transgene. Brightfield and fluorescence imaging revealed that while *vit-2::gfp* animals contained roughly half the number of embryos as wild-type animals, *adr-2(-);vit-2::gfp* animals contained a similar number to wild-type and *adr-2(-)* animals lacking the *vit-2::gfp* transgene (**Figure 1A**). To quantify embryo content in a larger sample size, an embryo counting assay was performed. The average number of embryos contained in the uterus of *adr-2(-);vit-2::gfp* animals was significantly greater than that of *vit-2::gfp* animals, but did not significantly differ from wild-type animals without the *vit-2::gfp* transgene (**Figure 1B**). The effect of *adr-2* on embryo content is specific to the *vit-2::gfp* transgenic background, as *adr-2(-)* animals did not show a significant difference in embryo content compared to wild-type animals (**Figure 1B**). To ensure that the restoration of fertility was not due to any background mutations in the *adr-2(ok735)* strain or the specific *adr-2* genetic lesion, the *vit-2::gfp* transgene was crossed into a second *adr-2* deletion mutant (*adr-2(uu28)* (Reich and others 2018)). A second deletion allele was used as attempts to create a transgenic rescue for *adr-2* have been unsuccessful, likely due to its native location in a six-gene operon. Similar to *adr-2(ok735)*, *adr-2(uu28);vit-2::gfp* animals had significantly greater embryo content than *vit-2::gfp* animals, but did not significantly differ from wild-type and *adr-2(uu28)* animals without the *vit-2::gfp* transgene (**Figure S1**). These results indicate that loss of *adr-2* is sufficient to rescue the embryo content of animals expressing the *vit-2::gfp* transgene.

To gain further insight into the differences in embryo content observed in *vit-2::gfp* and *adr-2(-);vit-2::gfp* animals, we tested whether these differences resulted from a difference in reproductive timing. To test this, the number of viable offspring produced by each strain during each day of reproductive adulthood was monitored. Egg-laying for all strains started, peaked, and ended on the same days, suggesting no significant changes in reproductive timing in adulthood (**Figure 1C**). With respect to total brood size over the six peak days of egg-laying, *adr-2(-);vit-2::gfp* animals had a significantly greater brood size compared to *vit-2::gfp* animals, and had a similar brood size to non-transgenic strains (**Figure 1D**). Furthermore, there was no significant difference between brood sizes of wild-type and *adr-2(-)* animals, confirming that the effect is transgene-specific. Taken together, these results indicate that the loss of *adr-2* is sufficient to rescue the fertility defects of animals expressing the *vit-2::gfp* transgene.

A screen for factors that affect vitellogenesis and embryo production

Considering that proximal oocytes and embryos in *vit-2::gfp* animals are fluorescent, and that the fertility defect results in fewer embryos contained within the uterus, we reasoned that fertility in *vit-2::gfp* animals could be estimated by measuring the fluorescence intensity of gravid worms. The COPAS SELECT (Union Biometrica) is a large particle sorter that can measure the length, density, and fluorescence intensity of large populations of individual animals. Sorting with COPAS instruments has been used previously to measure the impact of various chemicals on embryos within adult *C. elegans* (Shin and others 2019). To test this method, we used COPAS sorting to measure the fluorescence intensity of large populations of gravid *vit-2::gfp* and *adr-2(-);vit-2::gfp* animals. Synchronized *vit-2::gfp* animals and *adr-2(-);vit-2 gfp* animals were

allowed to develop for 60 hours prior to sorting. The length and density measures were used to restrict the analysis to adult animals, and the fluorescence values were averaged for each sorting run, which ranged from ~2000-5000 animals. The average fluorescence intensity of adult *adr-2(-);vit-2::gfp* animals was significantly higher than that of *vit-2::gfp* animals (**Figure 2A**), mirroring the embryo content and brood size of the strains (**Figure 1**).

Having determined a high-throughput method for measuring fertility by proxy, a reverse genetic screen was designed to identify regulators of fertility and vitellogenesis (**Figure 2B**). As RNA-level regulation has been shown to play important roles in germ cell development and regulation of fertility (Albarqi and Ryder 2022; Kimble and Crittenden 2007), we decided to focus our screen on RNA binding proteins (RBPs). As removal of *adr-2* rescues the fertility defect in the *vit-2::gfp* background, the *adr-2(-);vit-2::gfp* strain was used as a defect-corrected background for the screen. This allows us to identify RBPs that both negatively and positively affect fertility (**Figure 2B**). The *adr-2(-);vit-2::gfp* animals were synchronized and treated with RNAi against 255 RBPs that represent diverse classes of RBPs, including those that recognize single stranded RNA, such as the K Homology (KH) and RNA Recognition Motif (RRM) domains as well as those that recognize double-stranded RNA, such as the double-stranded RNA binding domain (dsRBD) (**Table S2)**. After 60 hours, animals were collected from each treatment and the average GFP fluorescence of each strain was measured using the COPAS SELECT, restricting the analysis to adult animals as specified above. Each experiment included a control group fed with bacteria expressing an empty RNAi vector and a control group treated with *gfp* RNAi. Average fluorescence values for each experimental treatment of ~2000-5000 animals were normalized to the average fluorescence value for the *adr-2(-);vit-2::gfp* animals treated with empty vector RNAi. Treatments that caused a 2.5-fold or greater change in fluorescence were selected as hits (**Figure S2A, Table S3).** Each hit was tested a second time (**Figure S2B, Table S4**), and hits that did not show a similar trend in both replicates were eliminated to allow for identification of only high-confidence regulators of vitellogenesis and/or fertility (**Figure 2C**). Of the 255 RBPs tested, 23 high-confidence regulators of vitellogenesis and embryo production were identified (**Figure 2C**), including 15 positive and 8 negative regulators. The RNAi vector for each high-confidence regulator was confirmed by Sanger sequencing. Importantly, several known regulators of fertility were captured in the screen (**Table S5**), including *gld-1* (Lee and Schedl 2010) and *puf-8* (Datla and others 2014).

Because the screen was performed in the *adr-2(-)* background, it is possible that the lack of *adr-2* could be required for the changes in fertility observed upon loss of the regulators. To investigate this possibility, *vit-2::gfp* animals were also subjected to RNAi with the high confidence regulators (**Table S4**). It is important to note that because the *vit-2::gfp* strain has low baseline fertility, it is unlikely to identify changes in GFP fluorescence as drastic as those seen in *adr-2(-);vit-2::gfp* animals, especially for factors that decrease fluorescence. Thus, we compared the general trend of fluorescence in *vit-2::gfp* animals to *adr-2(-);vit-2::gfp* animals (**Figure 2D**). For the majority of the RBPs (18/23), a similar change in GFP fluorescence compared to control was observed in both *vit-2::gfp* and *adr-2(-);vit-2::gfp* animals, suggesting the changes in fluorescence are independent of *adr-2*. The 5 other RBPs fell into one of two categories: those producing almost no difference in GFP fluorescence from controls in *vit-2::gfp* animals (*pabp-2* and *cgh-1*), and those that had an opposite effect on GFP fluorescence in *vit-2::gfp* animals compared to *adr-2(-);vit-2::gfp* animals (*sfa-1*, *csr-1*, and *sqd-1*) (**Figure 2D**). Because *pabp-2* RNAi caused decreased fluorescence in *adr-2(-);vit-2::gfp* animals, the lack of a significant change in GFP fluorescence in the *vit-2::gfp* animals may be attributable to the already lowered

fertility in this strain. However for *cgh-1* RNAi, which causes an increase in fluorescence in *adr-2(-);vit-2::gfp* animals, the lack of a similar increase in *vit-2::gfp* animals suggests a synthetic interaction between *cgh-1* and *adr-2*. Similarly, RNAi treatments for *sfa-1*, *csr-1*, and *sqd-1* showed a significant increase in GFP fluorescence in *adr-2(-)::vit-2::gfp* and a slight decrease in fluorescence in *vit-2::gfp* animals, suggesting potential synthetic interactions of *sfa-1*, *csr-1* and *sqd-1* with *adr-2*.

***Investigating potential synthetic interactions with* adr-2**

To further investigate the potential synthetic interactions of *adr-2* with *cgh-1*, *csr-1*, *sfa-1*, and *sqd-1*, embryo counting assays were performed on RNAi-treated animals. Both transgenic (*vit-2::gfp* and *adr-2(-);vit-2::gfp*) and non-transgenic (wild-type and *adr-2(-)*) strains were tested to differentiate effects specific to the transgenic background (**Figure 3A**). For all strains tested, the animals treated with control (empty vector) RNAi (**Figure 3A**) showed similar embryo counts to those observed when the animals were grown on standard media (**Figure 1B**), indicating that the RNAi methodology does not impact fertility. Animals treated with *cgh-1* RNAi contained no embryos in all strains tested (**Figure 3A,** top left panel). This is consistent with previous reports of sterility in *cgh-1(-)* animals (Audhya and others 2005). RNAi against *csr-1* caused approximately a two-fold reduction in embryo content compared to controls for each strain tested, although not significant in *vit-2::gfp* (**Figure 3A,** top right panel), consistent with previous reports of decreased fertility in *csr-1(-)* animals (Yigit and others 2006). Treatment with *sfa-1* RNAi did not significantly affect embryo counts in any of the strains tested (**Figure 3A,** bottom left panel). In contrast, *sqd-1* RNAi caused sterility (no embryos) in both wild-type and *vit-2::gfp* animals, but, intriguingly, had less severe defects in both *adr-2(-)* and *adr-2(-);vit-2::gfp* strains (**Figure 3A,** bottom right panel).

In all of these conditions, the embryo counts in *adr-2(-);vit-2::gfp* animals were lower than or equal to those in animals treated with control RNAi (**Figure 3A**). These data are in contrast to the COPAS detection, where, upon depletion of *cgh-1*, *csr-1*, *sfa-1* or *sqd-1*, the average fluorescence was higher than that observed with control RNAi (**Figure 2C**). To investigate the discrepancy between GFP fluorescence and embryo content, imaging was performed on *vit-2::gfp* and *adr-2(-);vit-2::gfp* worms treated with control (empty vector) RNAi and RNAi against each factor (**Figure 3B**). In focusing on the brightfield images, consistent with the embryo counting results (**Figure 3A**), the *vit-2::gfp* animals treated with control RNAi contain fewer embryos than *adr-2(-);vit-2::gfp* animals treated with control RNAi (top panels, **Figure 3B**). Consistent with the fertility defects observed upon *cgh-1*, *csr-1*, and *sqd-1* RNAi treatment (**Figure 3A**), both the *vit-2::gfp* and *adr-2(-);vit-2::gfp* animals treated with RNAi for *cgh-1*, *csr-1* or *sqd-1* contained fewer embryos than animals treated with control RNAi (second, third and fifth panels, **Figure 3B**). The embryo content appeared reduced in *vit-2::gfp* animals treated with *sfa-1* RNAi compared to *vit-2::gfp* animals treated with control RNAi, but *adr-2(-);vit-2::gfp* animals treated with *sfa-1* RNAi had a similar embryo content to animals treated with control RNAi (**Figure 3B**), consistent with embryo counting results (**Figure 3A,** bottom left panel).

When focusing on the fluorescence images, consistent with the COPAS GFP intensity data (**Figure 2A**) and the brightfield images, *adr-2(-);vit-2::gfp* animals treated with control RNAi have an increased number of GFP positive embryos compared to *vit-2::gfp* animals under the same treatment (**Figure 3B**, top panels). Strikingly, for the *adr-2(-);vit-2::gfp* animals treated with *cgh-1* RNAi, the GFP fluorescence was not restricted to the embryos and was observed

throughout the body cavity (**Figure 3B**, second panels on right). These data provide an explanation for the discrepancy between the embryo counting data (**Figure 3A**) and the observed increase in GFP fluorescence intensity using the COPAS instrument for *adr-2(-);vit-2::gfp* animals (**Figure 2C**). In contrast, there does not appear to be a strong increase in GFP fluorescence intensity in the *vit-2::gfp* animals treated with *cgh-1* RNAi (**Figure 3B**, second panels on left), which is consistent with the GFP fluorescence intensity observed using the COPAS instrument (**Figure 2D**). Similar results were observed for animals treated with *csr-1*, *sfa-1* and *sqd-1* RNAi (**Figure 3B**, third, fourth and fifth panels). Of note, alterations in yolk protein localization defects in animals treated with RNAi against *sfa-1* and *cgh-1* have been previously reported (Balklava and others 2007).

Together, these data suggest that the high GFP signal measured in the COPAS screen for *adr-2(-);vit-2::gfp* animals treated with RNAi against *cgh-1*, *csr-1*, *sfa-1* or *sqd-1* (**Figure 2C**) results not from a higher embryo content, but from accumulation of excess VIT-2::GFP in the body cavity. These data also confirm previous reports of lower fertility in animals depleted for *cgh-1*, *csr-1*, and *sqd-1* (Audhya and others 2005; Maeda and others 2001; Yigit and others 2006).

sqd-1 *and* adr-2 *coregulate thousands of transcripts*

An interesting result from the embryo counting assays performed above was the decrease in severity of fertility defects due to *sqd-1* RNAi in *adr-2* mutant strains compared to strains with wild-type *adr-2* expression (**Figure 3A**). This suggests that *adr-2* may contribute to the fertility defects observed in *sqd-1* RNAi animals. However, it is also possible that fertility is enhanced in the *adr-2(-)* background due to reduced efficiency of RNAi, leading to a higher expression of *sqd-1* mRNA in *adr-2(-)* animals treated with *sqd-1* RNAi than in wild-type animals. To rule out this possibility, quantitative real-time PCR was performed to measure *sqd-1* levels in total RNA isolated from wild-type and *adr-2(-)* animals treated with control (empty vector) or *sqd-1* RNAi. Importantly, both strains showed similar reduced levels of *sqd-1* mRNA when treated with *sqd-1* RNAi (**Figure S3**).

To further investigate the relationship between *adr-2* and *sqd-1*, RNA-sequencing was performed on young adult wild-type animals treated with either control (empty vector) or *sqd-1* RNAi and *adr-2(-)* animals treated with either control or *sqd-1* RNAi. To determine how *adr-2* and *sqd-1* affect gene expression, sequencing reads were aligned to the *C. elegans* reference genome and differential gene expression analysis was performed using DESeq2 (Love and others 2014). Compared to wild-type animals, loss of *adr-2* alone caused significant altered expression (padj ≤ 0.05) of only *adr-2* and no other genes (**Figure S4A, Table S6**), suggesting that loss of *adr-2* alone does not significantly affect the gene expression of any transcripts in young adult *C. elegans* at the whole worm level. In sharp contrast, RNA isolated from wild-type animals depleted of *sqd-1* exhibited misregulation of 8411 genes compared to RNA isolated from wild-type animals treated with control (empty vector) RNAi (**Figure 4A, Table S7**). However, when *sqd-1* was depleted from *adr-2(-)* animals, only 1412 genes were misregulated compared to control RNAi (**Figure 4B, Table S8**). These data suggest that the presence of *adr-2* may be required for the majority of altered gene expression upon loss of *sqd-1*. To test this possibility, the genes that were misregulated in *sqd-1* depleted animals in the presence and absence of *adr-2* were overlapped (**Figure 4C**). Loss of *adr-2* rescued the expression of 7104 of the 8411 genes affected by *sqd-1* RNAi, suggesting that, in the absence of *sqd-1*, these genes are misregulated via an ADR-2-dependent mechanism (**Figure 4C**). The majority of the *sqd-1* regulated genes

that are affected by *adr-2* fall into the category of genes downregulated upon depletion of *sqd-1* in wild-type animals (**Figure 4C)**. Expression changes of these genes in *adr-2(-)* animals treated with *sqd-1* RNAi show either no change or a slight reduction in expression compared to animals treated with control RNAi, but all show distinctly less misregulation than in wild-type animals (**Figure 4D**). Gene ontology analysis (Angeles-Albores and others 2018; Angeles-Albores and others 2016) of the 89 genes downregulated by depletion of *sqd-1* in both wild-type and *adr-2(-)* animals (**Tables S4, S5**) revealed only 4 significant ontologies: structural constituent of chromatin, protein heterodimerization activity, nucleosome, and P-body. In contrast, gene ontology analysis performed on the genes significantly downregulated in wild-type animals depleted of *sqd-1* compared to *adr-2(-)* animals depleted of *sqd-1* (**Table S9**) reveals enrichment for many gene ontologies related to fertility, including reproduction, oocyte differentiation, meiotic cell cycle, embryonic axis specification, and others (**Figure 4E**). Thus, rescue of the expression of these genes in *adr-2(-)* animals could potentially explain the rescue of fertility seen in these animals.

***Loss of* sqd-1 *causes defects in oogenesis, which are remediated by loss of* adr-2.**
Due to the sterility and misregulation of germline genes in animals depleted for *sqd-1*, we sought to explore the effects of loss of *sqd-1* on germline morphology. Germline dissection and DAPI staining were performed on wild-type and *adr-2(-)* animals treated with control and *sqd-1* RNAi. Both wild-type and *adr-2(-)* animals treated with control RNAi produced typical germline structures (Pazdernik and Schedl 2013), with many syncytial nuclei at the distal end of the germline, apparent germ cell culling around the bend of the gonad, and individual, cellularized oocytes in the proximal germline region (**Figure 5**, top row). Wild-type animals treated with *sqd-1* RNAi produced germlines that appeared normal at the distal end but did not form individual oocytes at the proximal end. Instead, many germ nuclei populate the proximal end and do not appear to progress through the final stages of oocyte differentiation, as evidenced by the lack of cellularization, cell growth, and correct chromosome conformation within the proximal germ nuclei (**Figure 5**, bottom left). Strikingly, when *sqd-1* RNAi is performed in *adr-2(-)* animals, the germlines do not show similar defects as the wild-type animals treated with *sqd-1* RNAi; instead, the germlines appear to proceed through oocyte and embryo production as normal (**Figure 5**, bottom right). These observations may explain why *adr-2(-)* animals treated with *sqd-1* RNAi are not sterile as wild-type animals treated with *sqd-1* RNAi are (**Figure 3A,** bottom right panel). Additionally, this restoration of germline defects is consistent with the remediation of gene expression for several germline genes in *adr-2(-)* animals treated with *sqd-1* RNAi compared to wild-type animals treated with *sqd-1* RNAi (**Figure 4**). Together these data suggest that coregulation of germline transcripts by *sqd-1* and *adr-2* ensures proper germline gene expression, leading to proper germline development and fertility.

Discussion
Here, we report the results of a reverse genetic screen to identify RBPs that regulate vitellogenesis and/or embryogenesis in *C. elegans*. This screen identified *sqd-1* as a regulator of embryogenesis based on the lack of embryos produced by animals treated with *sqd-1* RNAi, and that loss of *adr-2* rescues the infertility observed upon *sqd-1* depletion. Further investigation revealed that *adr-2* is necessary for the misregulation of thousands of genes that occur upon *sqd-1* depletion, as well as for defective oogenesis observed in animals depleted of *sqd-1*.

This study presents the first characterization of the effects of *sqd-1* on gene expression in *C. elegans* and, to our knowledge, the first global, whole-animal assessment of regulation of gene expression by Squid proteins. We identified 8411 transcripts that were significantly misexpressed in animals treated with *sqd-1* RNAi (**Figure 4A**). Previous studies in *Drosophila* and *C. tentans* have identified a handful of specific target RNAs subject to regulation of localization by Squid proteins (Clouse and others 2008; Goodrich and others 2004; Kelley 1993; Lall and others 1999; Norvell and others 1999; Visa and others 1996). Studies of the human orthologs of *sqd-1*, HNRNPAB and HNRNPDL, in human cancer cell lines have identified specific targets of gene expression regulation by HNRNPAB (Yang and others 2020) and the effects of HNRNPDL on the transcriptome more broadly (Li and others 2019).

Additionally, we show that the germlines from animals depleted for *sqd-1* have defects in oogenesis (**Figure 5**), which likely account for the infertility observed in animals subjected to *sqd-1* RNAi (**Figure 3A**). The lack of oocytes in adult animals subjected to *sqd-1* RNAi likely contributes greatly to the >8000 misregulated transcripts observed in these animals (**Figure 4A**). While further research is needed to pinpoint the molecular cause of these defects, the phenotype observed in animals treated with *sqd-1* RNAi suggests that germ cells are unable to differentiate into oocytes in the absence of *sqd-1*. In *Drosophila*, *squid* mutant embryo defects stem from the mislocalization of *gurken* mRNA; Gurken is an EGFR ligand whose dorsal-specific localization during later stages of oogenesis is necessary for proper embryo patterning (Norvell and others 1999). Similarly, it is possible that the sterility in *C. elegans* depleted of *sqd-1* could be a result of mislocalization of a specific mRNA target of SQD-1, which in turn leads to the misexpression of several downstream genes. Future studies aimed at identification of the direct binding targets of SQD-1 are needed to fully elucidate the mechanisms by which SQD-1 regulates germline gene expression. SQD-1 is known to physically interact with GLD-1, a regulator of germline patterning in *C. elegans* (Akay and others 2013), and *gld-1* mutants show a similar germline phenotype as animals depleted for *sqd-1*, with undifferentiated germ cells accumulating in the proximal germline region (Lee and Schedl 2001). Thus, it is possible that a shared target or targets of SQD-1 and GLD-1 is/are responsible for this phenotype.

Another interesting avenue for future inquiry is defining the molecular relationship between ADR-2 and SQD-1. This is particularly interesting given recent reports of genetic interaction between ADARs and hnRNPs in humans (Herzner and others 2021) and yeast (Garncarz and others 2013). The gene expression data presented here suggests ADR-2 may act uniquely in the absence *sqd-1* to affect gene expression, or that SQD-1 normally regulates targeting of transcripts by ADR-2. One potential mechanism by which SQD-1 could affect ADR-2 activity is through a physical interaction between the two factors. A previous immunoprecipitation (IP) coupled to mass spectrometry experiment performed in our lab identified SQD-1 as a physical interactor of ADR-2 (Rajendren 2020). To validate these data, an ADR-2 IP was performed in a strain expressing CRISPR-integrated V5::SQD-1 and 3XFLAG::ADR-2. Western blotting of the ADR-2 IP confirmed the presence of SQD-1, suggesting the two factors interact *in vivo* (**Figure S5**). In future studies, it will be interesting to explore whether SQD-1 and ADR-2 interact directly or via shared RNA targets, whether SQD-1 affects the binding target specificity of ADR-2, and whether the A-to-I editing activity of ADR-2 is regulated by SQD-1. By interrogating the effect of SQD-1 on ADR-2 activity, we can not only elucidate a novel regulatory relationship between SQD-1 and ADR-2, but also potentially determine the molecular cause of the oogenesis defects caused by loss of *sqd-1* and explore the broader role of ADR-2 in regulating oogenesis. To date, this is the first evidence that an ADAR

family member may play a role in gene expression in oogenic germline tissues. Testis-specific roles for deaminase-deficient ADAR family members, ADADs, have previously been identified (Islam and others 2023; Snyder and others 2020), and A-to-I editing has been reported in human ovaries (Tan and others 2017). In future studies, it would be of interest to assess the effects of ADARs on germline RNA regulation more globally.

In this study, we determined that loss of *adr-2* rescues the fertility defect of *vit-2::gfp* animals, suggesting that *adr-2* is necessary for these defects and may play a role in successful reproduction. The specific role of *adr-2* in restoring the *vit-2::gfp* fertility defect is currently unknown. Since ADARs have previously been implicated in transgene silencing (Knight and Bass 2002), one possibility could be that ADR-2 functions in wildtype animals to silence the *vit-2::gfp* transgene ultimately leading to decreased fertility. Discrepancies between our own measures of *vit-2* expression in *vit-2::gfp* animals and measures reported in other studies (Seah and others 2016), as well as the lack of available VIT-2 antibodies, have made it difficult to definitively assess total vitellogenin (i.e. endogenous and VIT-2::GFP) expression levels in these strains. While the cause of the fertility defect is still unknown, *adr-2(-);vit-2::gfp* animals can be used as a fertility-corrected vitellogenin reporter in future studies.

Using the defect-adjusted *adr-2(-);vit-2::gfp* animals as a reporter of embryo content, a high-throughput RNAi screen was performed and identified 23 RNA binding proteins that regulate vitellogenesis and/or embryo production in *C. elegans* by demonstrating that loss of these factors (via RNAi) causes changes in embryo production. While some of these are known regulators of germline development, many do not have well-described roles in vitellogenesis or embryogenesis (**Table S5**). Of the 23 RBPs, 11 have characterized molecular functions in oogenesis or embryogenesis that likely contribute to the fertility phenotypes identified in the screen (**Table S5**). The 12 remaining RBPs have come up in previous screens for factors affecting germline morphology (Green and others 2011; Updike and Strome 2009), germline differentiation and sex determination (Kalis and others 2010; Kerins and others 2010; Wang and others 2012), and receptor meditated endocytosis (Balklava and others 2007), as well as general RNAi-based phenotypic screens (Kamath and others 2003; Maeda and others 2001); however specific roles of these RBPs in embryogenesis are not yet described. We suggest that the *adr-2(-);vit-2::gfp* strain could be used in future studies as a method for interrogating the function of mutations within the RBPs. One limitation of this screen is the possibility that certain RBP regulators of fertility were not identified due to ineffective RNAi or the lack of RNAi feeding vectors in our collection for certain RBPs. While we tested 255 RBPs, recent estimates predict ~800 RBPs are present in *C. elegans* (Tamburino and others 2013). Thus, there almost certainly remain important RBPs for fertility that weren't identified in this screen. Additionally, the germline in particular relies on many redundant factors and pathways (Albarqi and Ryder 2022; Kimble and Crittenden 2007; Lee and Schedl 2006; Sundby and others 2021), which may mask identification of the role of a given RBP in the germline when assessed by individual depletion experiments.

One interesting observation from our study was the accumulation of VIT-2::GFP in the body cavity of animals treated with RNAi against *cgh-1*, *csr-1*, *sqd-1*, and *sfa-1* (**Figure 3B**). Despite the reduction (*cgh-1*, *csr-1*, *sqd-1*) or lack of change in (*sfa-1*) oocyte production in these conditions, we noted an increase in VIT-2::GFP content compared to control animals (**Figures 2C, 3A**). This type of accumulation has previously been seen in animals with defects in receptor-mediated endocytosis (RME), the process by which yolk proteins are imported into developing oocytes (Balklava and others 2007; Balklava and others 2016; Grant and Hirsh 1999). Depletion

of *cgh-1* and *sfa-1* have previously been associated with defects in RME (Balklava and others 2007), and it is likely that RME is disrupted when *sqd-1* or *csr-1* is absent as well. Previous studies have suggested that vitellogenin production is normally subject to regulation by signals from the germline, ensuring there is enough vitellogenin to load into the oocytes being produced (Balklava and others 2016; DePina and others 2011). However, if this communication is somehow altered, vitellogenin production could become uncoupled to oocyte production, leading to accumulation of vitellogenin in the body cavity (Balklava and others 2016). Thus, it is possible that *cgh-1*, *csr-1*, *sqd-1*, and *sfa-1* may play roles in the coupling of vitellogenin production to oocyte production, which would account for the accumulation of vitellogenin when these factors are lost. Interestingly, in addition to yolk, it was recently reported that extracellular double-stranded RNAs (dsRNAs) are imported into oocytes by RME (Marré and others 2016). In future studies, it would be interesting to determine whether the import of dsRNAs and thereby embryonic gene silencing is impacted by loss of *cgh-1*, *csr-1*, *sqd-1*, or *sfa-1*.

Data availability

Strains and plasmids are available upon request. Raw and processed high-throughput sequencing data generated in this study have been submitted to the NCBI Gene Expression Omnibus (GEO; https://www.ncbi.nlm.nih.gov/geo/) under accession number GSE244602.

Acknowledgements

The authors would like to acknowledge Christiane Hassel and the Indiana University Flow Cytometry Core Facility for the use and operation of the COPAS SELECT, the Indiana University Center for Genomics and Bioinformatics for running the high-throughput sequencing experiments, Dr. Scott Aoki (Indiana University School of Medicine) for his assistance with learning gonad extrusion and staining, the Indiana University Light Microscopy Imaging Center for the use of the Leia SP8 Confocal, and Dr. Lesley Weaver for her feedback on the micrographs presented in the manuscript. The authors would also like to acknowledge the members of the Hundley Lab for their feedback and assistance on this manuscript.

Funding

This work was supported in part by the National Institutes of Health/National Institute of General Medical Sciences [R01GM130759] awarded to H.A.H, including supplemental funding for diversifying the biomedical workforce [R01GM130759-05S1] (M.S.) and for equipment [R01GM130759-03S1], a National Institutes of Health/National Institute of General Medical Sciences [T32 GM131994] and the National Institutes of Health/National Institute of Child Health and Human Development [F31 HD110244-01] awarded to E.E., and the National Center for Advancing Translational Sciences, Clinical and Translational Sciences Award (Indiana University Medical Student Program for Research and Scholarship (IMPRS) to M.B.). Some strains were provided by the *Caenorhabditis* Genetics Center (CGC), which is funded by NIH Office of Research Infrastructure Programs [P40 OD010440].

Conflict of Interest

The authors declare no conflict of interest.

Author contributions:
Designed the experiments: E.E., H.A.H.
Created reagents: S.P. (HAH56 strain), E.E. (HAH51-55strains)
Performed the experiments: E.E., M.F. (secondary screen), M.B. (primary screen) M.S. (Co-IP)
Performed the bioinformatics analysis: E.E.
Wrote and edited the manuscript: E.E., H.A.H.

Figure Legends

Figure 1: Loss of *adr-2* rescues the fertility defects of *vit-2::gfp* animals. A) Brightfield and fluorescence images showing embryos in synchronized animals of the indicated genotypes. B) Embryo content of the indicated strains. Data represents 3 biological replicates, n=20 animals/replicate. Statistical significance was determined via ordinary one-way Anova; ns= not significant (cut-off $p \leq 0.05$), ** indicates $p \leq 0.01$. C-D) Brood size assay of the indicated strains where both daily offspring (C) and total brood size (D) were plotted. Data represents 2-4 biological replicates. Statistical significance was determined via ordinary one-way Anova; ns= not significant ($p > 0.05$), * indicates $p \leq 0.05$.

Figure 2: Screen for RNA binding proteins that impact vitellogenesis and embryo production. A) COPAS fluorescence quantification of synchronized *vit-2::gfp* and *adr-2(-);vit-2::gfp* worms. Data represents 7 biological replicates, ~2000-5000 worms per replicate. Statistical significance was determined via unpaired t-test; **** indicates $p \leq 0.0001$. B) Schematic of screen. Figure created with BioRender. C) High confidence regulators of vitellogenesis and embryo production. Based on results in **Figure S2A-B**. First replicate data is plotted (**Table S3**). D) Heat map showing fluorescence changes (compared to control RNAi) upon RNAi of each high-confidence regulator in *adr-2(-);vit-2::gfp* animals and *vit-2::gfp* animals. Secondary screen data is plotted (**Table S3**).

Figure 3: Effects of RNAi against *cgh-1*, *csr-1*, *sfa-1*, and *sqd-1* on embryo content and vitellogenin localization. A) Embryo content of the indicated strains treated with empty vector RNAi (indicated by RNAi: -) or RNAi against *cgh-1*, *csr-1*, *sfa-1*, or *sqd-1* (indicated by RNAi: + in the respective panels). Synchronized adult animals were placed individually in 20% bleach until the cuticles dissolved, and the remaining embryos from each worm were counted. Data represents 3-7 replicates per condition, 20 animals/replicate. Statistical significance was determined via one-way Anova; ns = not significant ($p > 0.05$), ** indicates $p \leq 0.01$, *** indicates $p \leq 0.001$, **** indicates $p \leq 0.0001$. B) Representative brightfield (left panel for each strain, treatment) and fluorescent (right panel for each strain, treatment) images of the indicated strains treated with empty vector (control), *cgh-1*, *csr-1*, *sfa-1*, or *sqd-1* RNAi. Scale bars = 100 μm.

Figure 4: Loss of *sqd-1* results in misexpression of thousands of genes in an *adr-2* dependent manner. A-B) Differential gene expression of A) wild-type animals treated with *sqd-1* RNAi compared to wild-type animals treated with control RNAi (data in **Table S7**) B) *adr-2(-)* animals treated with *sqd-1* RNAi compared to *adr-2(-)* animals treated with control RNAi (data in **Table S8**). Red points indicate significantly upregulated genes (padj ≤ 0.05), blue points indicate significantly downregulated genes (padj ≤ 0.05), gray points indicate genes that were not significantly differentially expressed (padj > 0.05). C) Overlap of genes differentially expressed

in wild-type animals treated with *sqd-1* RNAi with genes differentially expressed in *adr-2(-)* animals treated with *sqd-1* RNAi, compared to animals treated with control RNAi. D) Log_2 Fold Change for genes downregulated (padj ≤0.05) in wild-type animals treated with *sqd-1* RNAi compared to wild-type animals treated with control RNAi, shown alongside their corresponding Log_2 Fold Change expression values for *adr-2(-)* animals treated with *sqd-1* RNAi compared to *adr-2(-)* animals treated with control RNAi. Values are listed alongside Wormbase Gene ID in **Tables S4 and S5**. E) Gene Ontology Analysis of genes downregulated in wild-type animals treated with *sqd-1* RNAi compared to *adr-2(-)* animals treated with *sqd-1* RNAi.

Figure 5: Animals lacking *sqd-1* exhibit defects in oogenesis, which are remediated by loss of *adr-2*. Representative confocal images of dissected germlines from wild-type and *adr-2(-)* animals treated with control RNAi or *sqd-1* RNAi, stained with DAPI. Scale bars = 50 µm Dotted lines indicate proximal germline region.

Figure S1: A second *adr-2* mutant allele restores embryo count in *vit-2::gfp* animals. Embryo content of the indicated strains is plotted. Data represents 3 biological replicates, n=20 worms/replicate. Statistical significance was determined via ordinary one-way Anova; ns= not significant (p> 0.05) * indicates p≤0.05

Figure S2: Primary and Secondary screens for RNA Binding Proteins that impact vitellogenesis and embryo production. A) Primary screen results. *adr-2(-);vit-2::gfp* animals were fed with RNAi against 255 RNA binding proteins. Animals were collected and average GFP fluorescence in each population was measured using the COPAS select. Analysis was restricted to worms meeting length and density criteria for adult worms. Treatments causing no significant change (gray points), ≥2.5 fold increase (red points), and ≥2.5 fold decrease (blue points) in GFP fluorescence compared to positive control (empty vector RNAi) treated animals are plotted. n=2000-5000 animals per treatment. B) RNAi vectors that caused significant change in GFP levels in the primary screen (A) were tested a second time to eliminate unreproducible results (n=2000-5000 animals per replicate). Solid points indicate average fluorescence values for each RNAi treatment in the primary screening replicate (red= increased compared to control, blue= decreased compared to control). Open symbols indicate average fluorescence values for each RNAi treatment in second screening replicate (gray= no significant difference compared to control, red= increased compared to control, blue= decreased compared to control). Treatments whose second replicates showed the opposite patten from the primary replicate (*nuo-2*, *F55F8.2*, *rbd-1, ddx-17*) were not designated high-confidence regulators.

Figure S3: *sqd-1* RNAi efficiency is unaffected in *adr-2(-)* animals compared to wild-type. qPCR was performed to measure *sqd-1* mRNA in wild-type animals treated with control RNAi and *sqd-1* RNAi and *adr-2(-)* animals treated with control RNAi and *sqd-1* RNAi. Plotted expression values are normalized to *gpd-3* (housekeeping gene) expression. Data represents 3 biological replicates. Significance determined via unpaired t-test, ns= no significant difference (p> 0.05).

Figure S4: Differential gene expression analysis for wild-type and *adr-2(-)* animals treated with control or *sqd-1* RNAi. A) Differential gene expression of *adr-2(-)* animals treated with control RNAi compared to wild-type animals treated with control RNAi (data in **Table S6**). Blue points

indicate significantly downregulated genes (padj ≤0.05), gray points indicate genes that were not significantly differentially expressed (padj > 0.05). B) Log_2 Fold Change for genes upregulated (padj ≤0.05) in wild-type animals treated with *sqd-1* RNAi compared to wild-type animals treated with control RNAi, shown alongside their corresponding Log_2 Fold Change expression values for *adr-2(-)* animals treated with *sqd-1* RNAi compared to *adr-2(-)* animals treated with control RNAi. Values are listed alongside Wormbase Gene ID in Tables **S4 and S5**.

Figure S5: Co-IP for 3XFLAG::ADR-2 and V5::SQD-1. FLAG (top panels) and V5 (bottom panels) immunoblots. Blots represent 3 independent biological replicates of immunoprecipitation. For replicates 1 and 2, the input samples were loaded as 1% of the total IP (5mg). Replicate 1 had 8% of the total IP loaded for the ADR-2 blot and 92% loaded for the SQD-1 blot for both strains. Replicate 2 had 12% of the total IP loaded for the ADR-2 blot and 88% for the SQD-1 blot for both strains. For replicate 3, the input sample was loaded as 1.3% of the total IP, 10% of the IP was loaded for the ADR-2 blot and 90% for the SQD-1 blot for both strains.

Supplementary Tables:

Table S1: Oligonucleotides used in this study.

Table S2: RNAi feeding vectors used in screen for regulators of fertility. Related to **Figures 2-5, S2, S3**. Column A indicates RNAi vector number used in this study, Column B indicates the name of the gene targeted by each RNAi vector, Column C indicates the corresponding WormbaseID, Column D indicates the type and number of RNA binding domains in each gene. Column E contains a description of each RNAi feeding vector, and Column F contains the references for the RNA binding domain information in Column D. References: (Mistry and others 2021; Paysan-Lafosse and others 2023; Sigrist and others 2013; Tamburino and others 2013)

Table S3: Primary screen data- *adr-2(-);vit-2::gfp* animals (Related to **Figures S2** and **2C,D)**. Column A indicates RNAi vector ID as listed in **Table S2**. Column B indicates the gene target of each RNAi vector, Column C indicates the corresponding WormbaseID. Column D indicates the average Time of Flight (TOF) value measured by the COPAS SELECT, Column E indicates the average extinction (ext) value measured by the COPAS SELECT, and Column F indicates the ratio of average TOF over ext. Column G indicates the average GFP fluorescence measured by the COPAS SELECT, and Column H indicates the number of animals analyzed in each experiment. Columns J, K, and L indicate normalized values for GFP, TOF, and ext, respectively. Normalized values are calculated by dividing the average value for each RNAi vector by the average value for the control vector in each experiment. Normalized GFP values highlighted green indicate ≥2.5-fold decrease in GFP compared to control, values highlighted red indicate ≥ 2.5-fold increase in GFP compared to control.

Table S4: Secondary screen data (Related to **Figures S2** and **2C,D)**. First page contains data for *adr-2(-);vit-2::gfp* animals, second page contains data for *vit-2::gfp* animals. Column A indicates RNAi vector ID as listed in **Table S2**. Column B indicates the gene target of each RNAi vector, Column C indicates the corresponding WormbaseID, Column D indicates the average Time of

Flight (TOF) value measured by the COPAS SELECT, Column E indicates the average extinction (ext) value measured by the COPAS SELECT, and Column F indicates the ratio of average TOF over ext. Column G indicates the average GFP fluorescence measured by the COPAS SELECT, and Column H indicates the number of animals analyzed in each experiment. Columns J, K, and L indicate normalized values for GFP, TOF, and ext, respectively. Normalized values are calculated by dividing the average value for each RNAi vector by the average value for the control vector in each experiment. Normalized GFP values highlighted green indicate ≥2.5-fold decrease in GFP compared to control, values highlighted red indicate ≥ 2.5-fold increase in GFP compared to control, values highlighted yellow indicate fold changes ≤2.5. On first page, column N indicates the normalized GFP value from the primary screen (**Table S3**).

Table S5: Previously described germline roles and genome-wide screen hits for RBPs designated high-confidence regulators of fertility. Related to **Figures 2-5, S2**. References: (Balklava and others 2007; Barbee and Evans 2006; Barbee and others 2002; Elbaum-Garfinkle and others 2015; Francis and others 1995; Fujita and others 1998; Graham and others 1993; Green and others 2011; Hubert and Anderson 2009; Kalis and others 2010; Kamath and others 2003; Kerins and others 2010; Ko and others 2013; Maeda and others 2001; Navarro and others 2001; Singh and others 2017; Subramaniam and Seydoux 2003; Updike and Strome 2009; Wang and others 2012; Wedeles and others 2013)

Table S6: Differentially expressed genes in *adr-2(-)* animals treated with control RNAi compared to wild-type animals treated with control RNAi (Related to **Figure S3**). Column A indicates WormbaseID of each gene, Column B indicates corresponding gene name, Column C indicates $\log_2$fold change value from DESeq, Column D indicates pvalue from DESeq, Column E indicates padj from DESeq, Columns F-H indicate expression values from DESeq for each of three replicates of *adr-2(-)* animals treated with control RNAi, Columns I-K indicate expression values from DESeq for each of three replicates of wild-type animals treated with control RNAi.

Table S7: Differentially expressed genes in wild-type animals treated with *sqd-1* RNAi compared to wild-type animals treated with control RNAi (Related to **Figure 4**). First page contains all differentially expressed genes Padj ≤ 0.05. Second page contains genes downregulated in wild-type animals treated with *sqd-1* RNAi compared to wild-type animals treated with control RNAi (Padj ≤0.05). Third page contains genes upregulated in wild-type animals treated with *sqd-1* RNAi compared to wild-type animals treated with control RNAi (Padj ≤0.05). For each page, Column A indicates WormbaseID of each gene, Column B indicates corresponding gene name, Column C indicates $\log_2$fold change value from DESeq, Column D indicates pvalue from DESeq, Column E indicates padj from DESeq, Columns F-H indicate expression values from DESeq for each of three replicates of wild-type animals treated with *sqd-1* RNAi, Columns I-K indicate expression values from DESeq for each of three replicates of wild-type animals treated with control RNAi.

Table S8: Differentially expressed genes in *adr-2(-)* animals treated with *sqd-1* RNAi compared to *adr-2(-)* animals treated with control RNAi (Related to **Figure 4**). First page contains all differentially expressed genes Padj ≤ 0.05. Second page contains genes downregulated in *adr-2(-*

) animals treated with *sqd-1* RNAi compared to *adr-2(-)* animals treated with control RNAi (Padj ≤0.05). Third page contains genes upregulated in *adr-2(-)* animals treated with *sqd-1* RNAi compared to *adr-2(-)* animals treated with control RNAi (Padj ≤0.05). For each page, Column A indicates WormbaseID of each gene, Column B indicates corresponding gene name, Column C indicates $\log_2$fold change value from DESeq, Column D indicates pvalue from DESeq, Column E indicates padj from DESeq, Columns F-H indicate expression values from DESeq for each of three replicates of *adr-2(-)* animals treated with *sqd-1* RNAi, Columns I-K indicate expression values from DESeq for each of three replicates of *adr-2(-)* animals treated with control RNAi.

Table S9: Differentially expressed genes in *adr-2(-)* animals treated with *sqd-1* RNAi compared to wild-type animals treated with *sqd-1* RNAi (Related to **Figure 4E**). First page contains all differentially expressed genes Padj ≤ 0.05. Second page contains genes downregulated in *adr-2(-)* animals treated with *sqd-1* RNAi compared to wild-type animals treated with *sqd-1* RNAi (Padj ≤0.05). Third page contains genes upregulated in *adr-2(-)* animals treated with *sqd-1* RNAi compared to wild-type animals treated with *sqd-1* RNAi (Padj ≤0.05). For each page, Column A indicates WormbaseID of each gene, Column B indicates corresponding gene name, Column C indicates $\log_2$fold change value from DESeq, Column D indicates pvalue from DESeq, Column E indicates padj from DESeq, Columns F-H indicate expression values from DESeq for each of three replicates of *adr-2(-)* animals treated with *sqd-1* RNAi, Columns I-K indicate expression values from DESeq for each of three replicates of wild-type animals treated with *sqd-1* RNAi.

References

Akay A, Craig A, Lehrbach N, Larance M, Pourkarimi E, Wright JE, Lamond A, Miska E, Gartner A. 2013. RNA-binding protein GLD-1/quaking genetically interacts with the mir-35 and the let-7 miRNA pathways in Caenorhabditis elegans. Open Biol 3(11):130151.

Albarqi MMY, Ryder SP. 2022. The role of RNA-binding proteins in orchestrating germline development in *Caenorhabditis elegans*. Front Cell Dev Biol 10:1094295.

Angeles-Albores D, Lee R, Chan J, Sternberg P. 2018. Two new functions in the WormBase Enrichment Suite. MicroPubl Biol 2018.

Angeles-Albores D, N Lee RY, Chan J, Sternberg PW. 2016. Tissue enrichment analysis for C. elegans genomics. BMC Bioinformatics 17(1):366.

Arribere JA, Kuroyanagi H, Hundley HA. 2020. mRNA Editing, Processing and Quality Control in *Caenorhabditis elegans*. Genetics 215(3):531-568.

Audhya A, Hyndman F, McLeod IX, Maddox AS, Yates JR, Desai A, Oegema K. 2005. A complex containing the Sm protein CAR-1 and the RNA helicase CGH-1 is required for embryonic cytokinesis in Caenorhabditis elegans. J Cell Biol 171(2):267-79.

Bachorik JL, Kimble J. 2005. Redundant control of the Caenorhabditis elegans sperm/oocyte switch by PUF-8 and FBF-1, two distinct PUF RNA-binding proteins. Proc Natl Acad Sci U S A 102(31):10893-7.

Balklava Z, Pant S, Fares H, Grant BD. 2007. Genome-wide analysis identifies a general requirement for polarity proteins in endocytic traffic. Nat Cell Biol 9(9):1066-73.

Balklava Z, Rathnakumar ND, Vashist S, Schweinsberg PJ, Grant BD. 2016. Linking Gene Expression in the Intestine to Production of Gametes Through the Phosphate Transporter PITR-1 in Caenorhabditis elegans. Genetics 204(1):153-62.
Barbee SA, Evans TC. 2006. The Sm proteins regulate germ cell specification during early C. elegans embryogenesis. Dev Biol 291(1):132-43.
Barbee SA, Lublin AL, Evans TC. 2002. A novel function for the Sm proteins in germ granule localization during C. elegans embryogenesis. Curr Biol 12(17):1502-6.
Clouse KN, Ferguson SB, Schüpbach T. 2008. Squid, Cup, and PABP55B function together to regulate gurken translation in Drosophila. Dev Biol 313(2):713-24.
Datla US, Scovill NC, Brokamp AJ, Kim E, Asch AS, Lee MH. 2014. Role of PUF-8/PUF protein in stem cell control, sperm-oocyte decision and cell fate reprogramming. J Cell Physiol 229(10):1306-11.
Deffit SN, Yee BA, Manning AC, Rajendren S, Vadlamani P, Wheeler EC, Domissy A, Washburn MC, Yeo GW, Hundley HA. 2017. The *C. elegans* neural editome reveals an ADAR target mRNA required for proper chemotaxis. eLife.
DePina AS, Iser WB, Park SS, Maudsley S, Wilson MA, Wolkow CA. 2011. Regulation of Caenorhabditis elegans vitellogenesis by DAF-2/IIS through separable transcriptional and posttranscriptional mechanisms. BMC Physiol 11:11.
Dhakal A, Salim C, Skelly M, Amichan Y, Lamm AT, Hundley HA. 2023. ADARs regulate cuticle collagen expression to promote survival to pathogen infection. bioRxiv:2023.05.03.539277.
Dowen RH, Ahmed S. 2019. Maternal Inheritance: Longevity Programs Nourish Progeny via Yolk. Curr Biol 29(15):R748-R751.
Elbaum-Garfinkle S, Kim Y, Szczepaniak K, Chen CC, Eckmann CR, Myong S, Brangwynne CP. 2015. The disordered P granule protein LAF-1 drives phase separation into droplets with tunable viscosity and dynamics. Proc Natl Acad Sci U S A 112(23):7189-94.
Erdmann EA, Abraham O, Hundley HA. 2022. *Caenorhabditis elegans* expressing a Vitellogenin::GFP fusion protein show reduced embryo content and brood size. MicroPubl Biol 2022.
Erdmann EA, Mahapatra A, Mukherjee P, Yang B, Hundley HA. 2021. To protect and modify double-stranded RNA - the critical roles of ADARs in development, immunity and oncogenesis. Crit Rev Biochem Mol Biol 56(1):54-87.
Ezcurra M, Benedetto A, Sornda T, Gilliat AF, Au C, Zhang Q, van Schelt S, Petrache AL, Wang H, Guardia Y et al. . 2018. C. elegans Eats Its Own Intestine to Make Yolk Leading to Multiple Senescent Pathologies. Curr Biol 28(20):3352.
Finger DS, Williams AE, Holt VV, Ables ET. 2023. Novel roles for RNA binding proteins squid, hephaesteus, and Hrb27C in Drosophila oogenesis. Dev Dyn 252(3):415-428.
Francis R, Barton MK, Kimble J, Schedl T. 1995. gld-1, a tumor suppressor gene required for oocyte development in Caenorhabditis elegans. Genetics 139(2):579-606.
Fujita M, Kawano T, Terashima K, Tanaka Y, Sakamoto H. 1998. Expression of spliceosome-associated protein 49 is required for early embryogenesis in Caenorhabditis elegans. Biochem Biophys Res Commun 253(1):80-4.
Garncarz W, Tariq A, Handl C, Pusch O, Jantsch MF. 2013. A high-throughput screen to identify enhancers of ADAR-mediated RNA-editing. RNA Biol 10(2):192-204.
Gems D, Kern CC, Nour J, Ezcurra M. 2021. Reproductive Suicide: Similar Mechanisms of Aging in. Front Cell Dev Biol 9:688788.

Ghanta KS, Ishidate T, Mello CC. 2021. Microinjection for precision genome editing in. STAR Protoc 2(3):100748.
Goldeck M, Gopal A, Jantsch MF, Mansouri Khosravi HR, Rajendra V, Vesely C. 2022. How RNA editing keeps an I on physiology. Am J Physiol Cell Physiol 323(5):C1496-C1511.
Goodrich JS, Clouse KN, Schüpbach T. 2004. Hrb27C, Sqd and Otu cooperatively regulate gurken RNA localization and mediate nurse cell chromosome dispersion in Drosophila oogenesis. Development 131(9):1949-58.
Graham PL, Schedl T, Kimble J. 1993. More mog genes that influence the switch from spermatogenesis to oogenesis in the hermaphrodite germ line of Caenorhabditis elegans. Dev Genet 14(6):471-84.
Grant B, Hirsh D. 1999. Receptor-mediated endocytosis in the Caenorhabditis elegans oocyte. Mol Biol Cell 10(12):4311-26.
Green RA, Kao HL, Audhya A, Arur S, Mayers JR, Fridolfsson HN, Schulman M, Schloissnig S, Niessen S, Laband K et al. . 2011. A high-resolution C. elegans essential gene network based on phenotypic profiling of a complex tissue. Cell 145(3):470-82.
Herzner AM, Khan Z, Van Nostrand EL, Chan S, Cuellar T, Chen R, Pechuan-Jorge X, Komuves L, Solon M, Modrusan Z et al. . 2021. ADAR and hnRNPC deficiency synergize in activating endogenous dsRNA-induced type I IFN responses. J Exp Med 218(9).
Hubert A, Anderson P. 2009. The C. elegans sex determination gene laf-1 encodes a putative DEAD-box RNA helicase. Dev Biol 330(2):358-67.
Hundley HA, Krauchuk AA, Bass BL. 2008. C. elegans and H. sapiens mRNAs with edited 3' UTRs are present on polysomes. RNA 14(10):2050-60.
Islam KN, Ajao A, Venkataramani K, Rivera J, Pathania S, Henke K, Siegfried KR. 2023. The RNA-binding protein Adad1 is necessary for germ cell maintenance and meiosis in zebrafish. PLoS Genet 19(8):e1010589.
Jordan JM, Hibshman JD, Webster AK, Kaplan REW, Leinroth A, Guzman R, Maxwell CS, Chitrakar R, Bowman EA, Fry AL et al. . 2019. Insulin/IGF Signaling and Vitellogenin Provisioning Mediate Intergenerational Adaptation to Nutrient Stress. Curr Biol 29(14):2380-2388.e5.
Kalis AK, Kroetz MB, Larson KM, Zarkower D. 2010. Functional genomic identification of genes required for male gonadal differentiation in Caenorhabditis elegans. Genetics 185(2):523-35.
Kamath RS, Fraser AG, Dong Y, Poulin G, Durbin R, Gotta M, Kanapin A, Le Bot N, Moreno S, Sohrmann M et al. . 2003. Systematic functional analysis of the Caenorhabditis elegans genome using RNAi. Nature 421(6920):231-7.
Kelley RL. 1993. Initial organization of the Drosophila dorsoventral axis depends on an RNA-binding protein encoded by the squid gene. Genes Dev 7(6):948-60.
Kerins JA, Hanazawa M, Dorsett M, Schedl T. 2010. PRP-17 and the pre-mRNA splicing pathway are preferentially required for the proliferation versus meiotic development decision and germline sex determination in Caenorhabditis elegans. Dev Dyn 239(5):1555-72.
Kern CC, Townsend S, Salzmann A, Rendell NB, Taylor GW, Comisel RM, Foukas LC, Bähler J, Gems D. 2021. C. elegans feed yolk to their young in a form of primitive lactation. Nat Commun 12(1):5801.

Kim S, Govindan JA, Tu ZJ, Greenstein D. 2012. SACY-1 DEAD-Box helicase links the somatic control of oocyte meiotic maturation to the sperm-to-oocyte switch and gamete maintenance in Caenorhabditis elegans. Genetics 192(3):905-28.
Kim W, Underwood RS, Greenwald I, Shaye DD. 2018. OrthoList 2: A New Comparative Genomic Analysis of Human and. Genetics 210(2):445-461.
Kimble J, Crittenden SL. 2007. Controls of germline stem cells, entry into meiosis, and the sperm/oocyte decision in Caenorhabditis elegans. Annu Rev Cell Dev Biol 23:405-33.
Kimble J, Sharrock WJ. 1983. Tissue-specific synthesis of yolk proteins in Caenorhabditis elegans. Dev Biol 96(1):189-96.
Knight SW, Bass BL. 2002. The role of RNA editing by ADARs in RNAi. Mol Cell 10(4):809-17.
Ko S, Kawasaki I, Shim YH. 2013. PAB-1, a Caenorhabditis elegans poly(A)-binding protein, regulates mRNA metabolism in germline by interacting with CGH-1 and CAR-1. PLoS One 8(12):e84798.
Lall S, Francis-Lang H, Flament A, Norvell A, Schüpbach T, Ish-Horowicz D. 1999. Squid hnRNP protein promotes apical cytoplasmic transport and localization of Drosophila pair-rule transcripts. Cell 98(2):171-80.
Lee MH, Schedl T. 2001. Identification of in vivo mRNA targets of GLD-1, a maxi-KH motif containing protein required for C. elegans germ cell development. Genes Dev 15(18):2408-20.
Lee MH, Schedl T. 2006. RNA-binding proteins. WormBook:1-13.
Lee MH, Schedl T. 2010. C. elegans star proteins, GLD-1 and ASD-2, regulate specific RNA targets to control development. Adv Exp Med Biol 693:106-22.
Li RZ, Hou J, Wei Y, Luo X, Ye Y, Zhang Y. 2019. hnRNPDL extensively regulates transcription and alternative splicing. Gene 687:125-134.
Love MI, Huber W, Anders S. 2014. Moderated estimation of fold change and dispersion for RNA-seq data with DESeq2. Genome Biol 15(12):550.
Maeda I, Kohara Y, Yamamoto M, Sugimoto A. 2001. Large-scale analysis of gene function in Caenorhabditis elegans by high-throughput RNAi. Curr Biol 11(3):171-6.
Mahapatra A, Dhakal A, Noguchi A, Vadlamani P, Hundley HA. 2023. ADAR-mediated regulation of PQM-1 expression in neurons impacts gene expression throughout C. elegans and regulates survival from hypoxia. PLoS Biol 21(9):e3002150.
Marré J, Traver EC, Jose AM. 2016. Extracellular RNA is transported from one generation to the next in Caenorhabditis elegans. Proc Natl Acad Sci U S A 113(44):12496-12501.
Mistry J, Chuguransky S, Williams L, Qureshi M, Salazar GA, Sonnhammer ELL, Tosatto SCE, Paladin L, Raj S, Richardson LJ et al. . 2021. Pfam: The protein families database in 2021. Nucleic Acids Res 49(D1):D412-D419.
Navarro RE, Shim EY, Kohara Y, Singson A, Blackwell TK. 2001. cgh-1, a conserved predicted RNA helicase required for gametogenesis and protection from physiological germline apoptosis in C. elegans. Development 128(17):3221-32.
Nguyen-Chi M, Morello D. 2011. RNA-binding proteins, RNA granules, and gametes: is unity strength? Reproduction 142(6):803-17.
Norvell A, Kelley RL, Wehr K, Schüpbach T. 1999. Specific isoforms of squid, a Drosophila hnRNP, perform distinct roles in Gurken localization during oogenesis. Genes Dev 13(7):864-76.

Park Y, O'Rourke S, Taki FA, Alfhili MA, Lee MH. 2020. Dose-Dependent Effects of GLD-2 and GLD-1 on Germline Differentiation and Dedifferentiation in the Absence of PUF-8. Front Cell Dev Biol 8:5.

Paysan-Lafosse T, Blum M, Chuguransky S, Grego T, Pinto BL, Salazar GA, Bileschi ML, Bork P, Bridge A, Colwell L et al. . 2023. InterPro in 2022. Nucleic Acids Res 51(D1):D418-D427.

Pazdernik N, Schedl T. 2013. Introduction to germ cell development in Caenorhabditis elegans. Adv Exp Med Biol 757:1-16.

Priti A, Subramaniam K. 2015. PUF-8 Functions Redundantly with GLD-1 to Promote the Meiotic Progression of Spermatocytes in Caenorhabditis elegans. G3 (Bethesda) 5(8):1675-84.

Rajendren S. 2020. Molecular Mechanisms to Regulate A-to-I RNA Editing in *Caenorhabditis elegans* [Ph.D. dissertation]. Indiana University. p. 215.

Reich DP, Tyc KM, Bass BL. 2018. *C. elegans* ADARs antagonize silencing of cellular dsRNAs by the antiviral RNAi pathway. Genes & Development. p. 271-282.

Rosario R, Childs AJ, Anderson RA. 2017. RNA-binding proteins in human oogenesis: Balancing differentiation and self-renewal in the female fetal germline. Stem Cell Res 21:193-201.

Savva YA, Rieder LE, Reenan RA. 2012. The ADAR protein family. Genome Biol 13(12):252.

Scheckel C, Gaidatzis D, Wright JE, Ciosk R. 2012. Genome-wide analysis of GLD-1-mediated mRNA regulation suggests a role in mRNA storage. PLoS Genet 8(5):e1002742.

Seah NE, de Magalhaes Filho CD, Petrashen AP, Henderson HR, Laguer J, Gonzalez J, Dillin A, Hansen M, Lapierre LR. 2016. Autophagy-mediated longevity is modulated by lipoprotein biogenesis. Autophagy 12(2):261-72.

Seydoux G, Braun RE. 2006. Pathway to totipotency: lessons from germ cells. Cell 127(5):891-904.

Shaye DD, Greenwald I. 2011. OrthoList: a compendium of C. elegans genes with human orthologs. PLoS One 6(5):e20085.

Shin N, Cuenca L, Karthikraj R, Kannan K, Colaiácovo MP. 2019. Assessing effects of germline exposure to environmental toxicants by high-throughput screening in C. elegans. PLoS Genet 15(2):e1007975.

Sigrist CJ, de Castro E, Cerutti L, Cuche BA, Hulo N, Bridge A, Bougueleret L, Xenarios I. 2013. New and continuing developments at PROSITE. Nucleic Acids Res 41(Database issue):D344-7.

Singh KD, Zheng X, Milstein S, Keller M, Roschitzki B, Grossmann J, Hengartner MO. 2017. Differential regulation of germ line apoptosis and germ cell differentiation by CPEB family members in C. elegans. PLoS One 12(7):e0182270.

Snyder E, Chukrallah L, Seltzer K, Goodwin L, Braun RE. 2020. ADAD1 and ADAD2, testis-specific adenosine deaminase domain-containing proteins, are required for male fertility. Sci Rep 10(1):11536.

Sornda T, Ezcurra M, Kern C, Galimov ER, Au C, de la Guardia Y, Gems D. 2019. Production of YP170 Vitellogenins Promotes Intestinal Senescence in Caenorhabditis elegans. J Gerontol A Biol Sci Med Sci 74(8):1180-1188.

Spike CA, Coetzee D, Eichten C, Wang X, Hansen D, Greenstein D. 2014. The TRIM-NHL protein LIN-41 and the OMA RNA-binding proteins antagonistically control the

prophase-to-metaphase transition and growth of Caenorhabditis elegans oocytes. Genetics 198(4):1535-58.
Subramaniam K, Seydoux G. 2003. Dedifferentiation of primary spermatocytes into germ cell tumors in C. elegans lacking the pumilio-like protein PUF-8. Curr Biol 13(2):134-9.
Sundby AE, Molnar RI, Claycomb JM. 2021. Connecting the Dots: Linking Caenorhabditis elegans Small RNA Pathways and Germ Granules. Trends Cell Biol 31(5):387-401.
Tamburino AM, Ryder SP, Walhout AJ. 2013. A compendium of Caenorhabditis elegans RNA binding proteins predicts extensive regulation at multiple levels. G3 (Bethesda) 3(2):297-304.
Tan MH, Li Q, Shanmugam R, Piskol R, Kohler J, Young AN, Liu KI, Zhang R, Ramaswami G, Ariyoshi K et al. . 2017. Dynamic landscape and regulation of RNA editing in mammals. Nature 550(7675):249-254.
Tonkin LA, Saccomanno L, Morse DP, Brodigan T, Krause M, Bass BL. 2002. RNA editing by ADARs is important for normal behavior in Caenorhabditis elegans. EMBO J 21(22):6025-35.
Updike DL, Strome S. 2009. A genomewide RNAi screen for genes that affect the stability, distribution and function of P granules in Caenorhabditis elegans. Genetics 183(4):1397-419.
Van Rompay L, Borghgraef C, Beets I, Caers J, Temmerman L. 2015. New genetic regulators question relevance of abundant yolk protein production in C. elegans. Sci Rep 5:16381.
Visa N, Alzhanova-Ericsson AT, Sun X, Kiseleva E, Björkroth B, Wurtz T, Daneholt B. 1996. A pre-mRNA-binding protein accompanies the RNA from the gene through the nuclear pores and into polysomes. Cell 84(2):253-64.
Wang C, Wilson-Berry L, Schedl T, Hansen D. 2012. TEG-1 CD2BP2 regulates stem cell proliferation and sex determination in the C. elegans germ line and physically interacts with the UAF-1 U2AF65 splicing factor. Dev Dyn 241(3):505-21.
Wang X, Ellenbecker M, Hickey B, Day NJ, Osterli E, Terzo M, Voronina E. 2020. Antagonistic control of Caenorhabditis elegans germline stem cell proliferation and differentiation by PUF proteins FBF-1 and FBF-2. Elife 9.
Wedeles CJ, Wu MZ, Claycomb JM. 2013. Protection of germline gene expression by the C. elegans Argonaute CSR-1. Dev Cell 27(6):664-71.
Yang Y, Chen Q, Piao HY, Wang B, Zhu GQ, Chen EB, Xiao K, Zhou ZJ, Shi GM, Shi YH et al. . 2020. HNRNPAB-regulated lncRNA-ELF209 inhibits the malignancy of hepatocellular carcinoma. Int J Cancer 146(1):169-180.
Yigit E, Batista PJ, Bei Y, Pang KM, Chen CC, Tolia NH, Joshua-Tor L, Mitani S, Simard MJ, Mello CC. 2006. Analysis of the C. elegans Argonaute family reveals that distinct Argonautes act sequentially during RNAi. Cell 127(4):747-57.
Yoon DS, Alfhili MA, Friend K, Lee MH. 2017. MPK-1/ERK regulatory network controls the number of sperm by regulating timing of sperm-oocyte switch in C. elegans germline. Biochem Biophys Res Commun 491(4):1077-1082.
Zanetti S, Grinschgl S, Meola M, Belfiore M, Rey S, Bianchi P, Puoti A. 2012. The sperm-oocyte switch in the C. elegans hermaphrodite is controlled through steady-state levels of the fem-3 mRNA. RNA 18(7):1385-94.

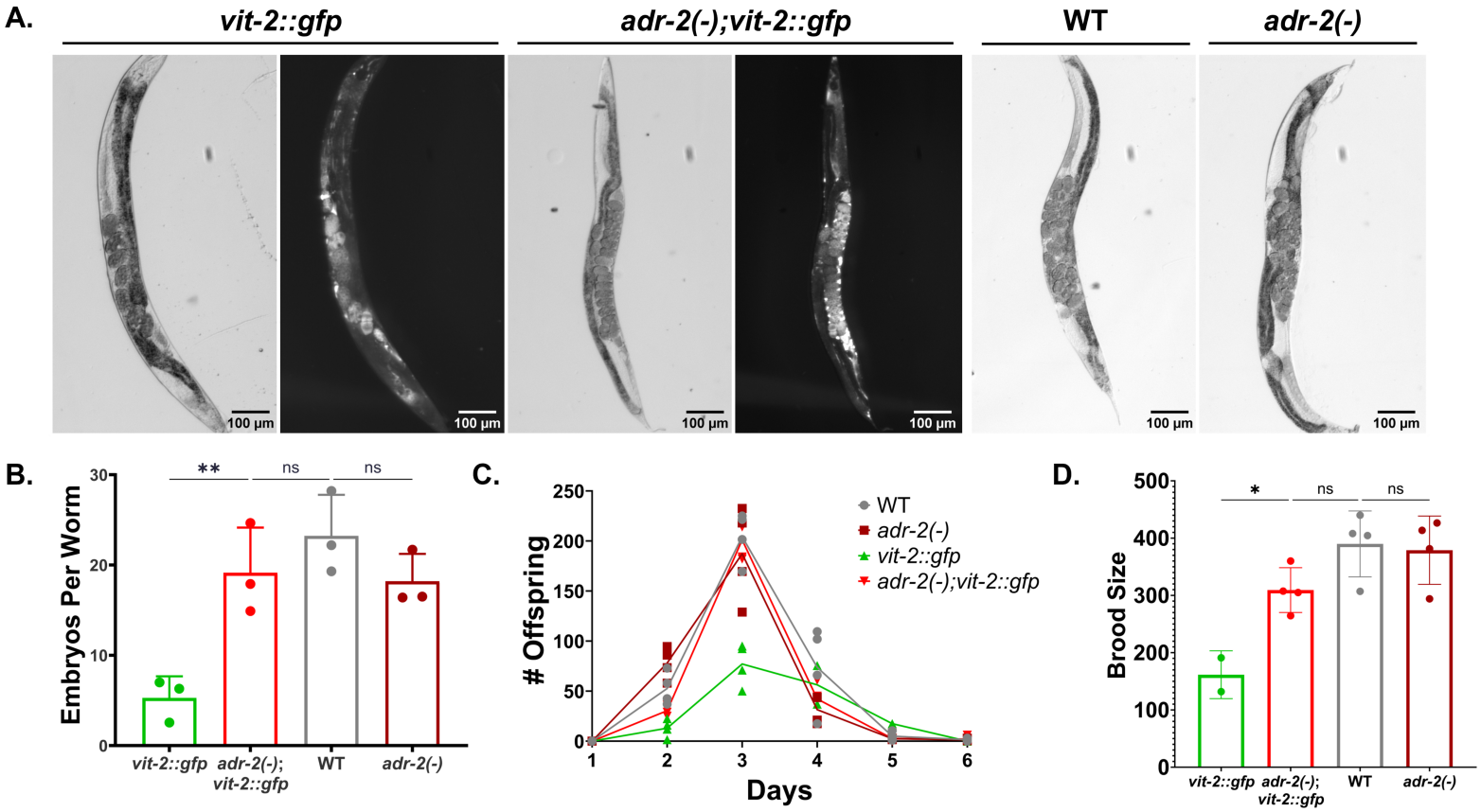
A.
vit-2::gfp
adr-2(-);vit-2::gfp
WT
adr-2(-)
100 µm
B.
Embryos Per Worm
**
ns
ns
vit-2::gfp
adr-2(-); vit-2::gfp
WT
adr-2(-)
C.
Offspring
Days
WT
adr-2(-)
vit-2::gfp
adr-2(-);vit-2::gfp
D.
Brood Size
*
ns
ns
vit-2::gfp
adr-2(-); vit-2::gfp
WT
adr-2(-)

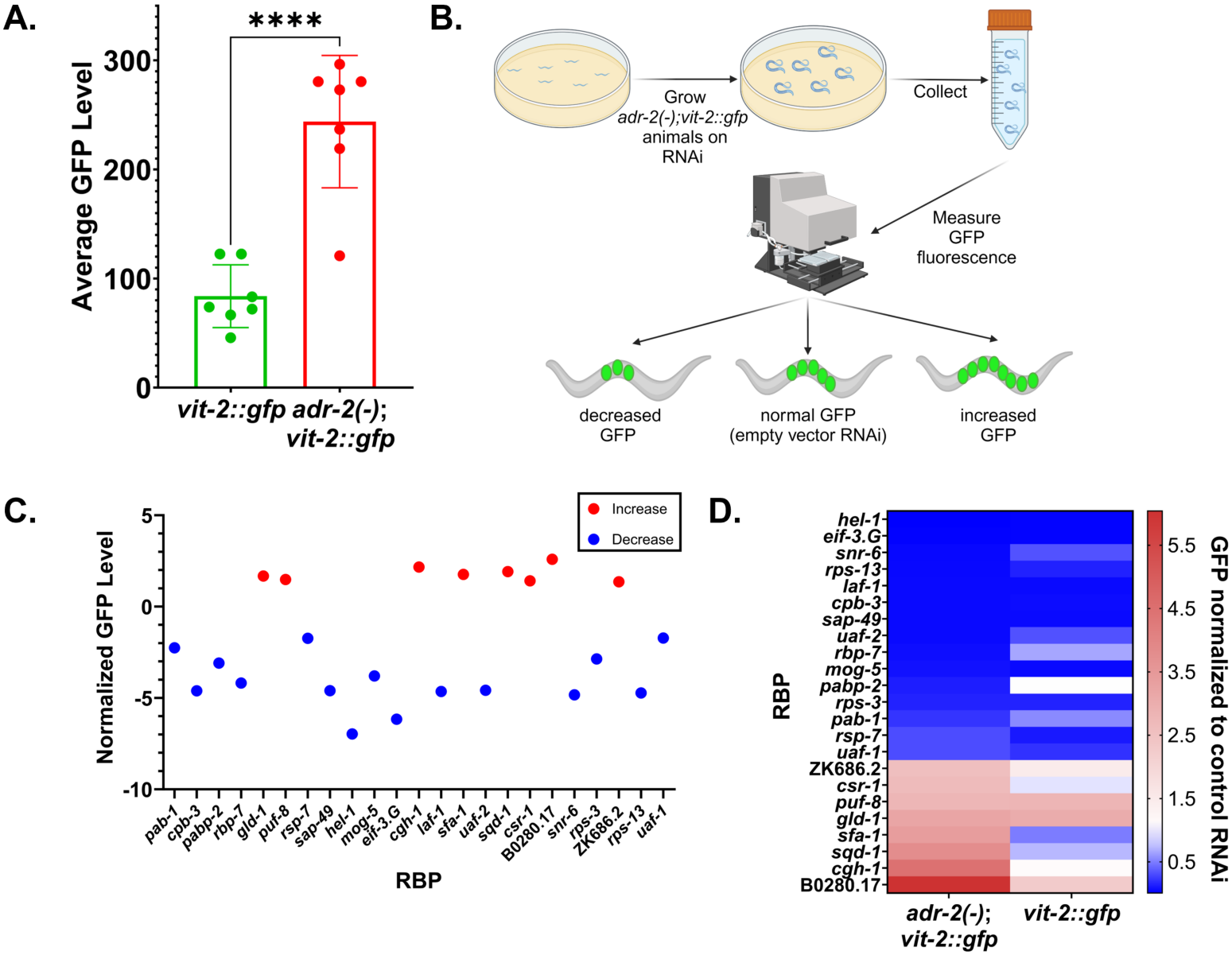
A.
****
Average GFP Level
300
200
100
0
vit-2::gfp
adr-2(-); vit-2::gfp
B.
Grow adr-2(-);vit-2::gfp animals on RNAi
Collect
Measure GFP fluorescence
decreased GFP
normal GFP (empty vector RNAi)
increased GFP
C.
Increase
Decrease
Normalized GFP Level
5
0
-5
-10
pab-1
cpb-3
pabp-2
rbp-7
gld-1
puf-8
rsp-7
sap-49
hel-1
mog-5
eif-3.G
cgh-1
laf-1
sfa-1
uaf-2
sqd-1
csr-1
B0280.17
snr-6
rps-3
ZK686.2
rps-13
uaf-1
RBP
D.
hel-1
eif-3.G
snr-6
rps-13
laf-1
cpb-3
sap-49
uaf-2
rbp-7
mog-5
pabp-2
rps-3
pab-1
rsp-7
uaf-1
ZK686.2
csr-1
puf-8
gld-1
sfa-1
sqd-1
cgh-1
B0280.17
RBP
adr-2(-); vit-2::gfp
vit-2::gfp
5.5
4.5
3.5
2.5
1.5
0.5
GFP normalized to control RNAi

A.

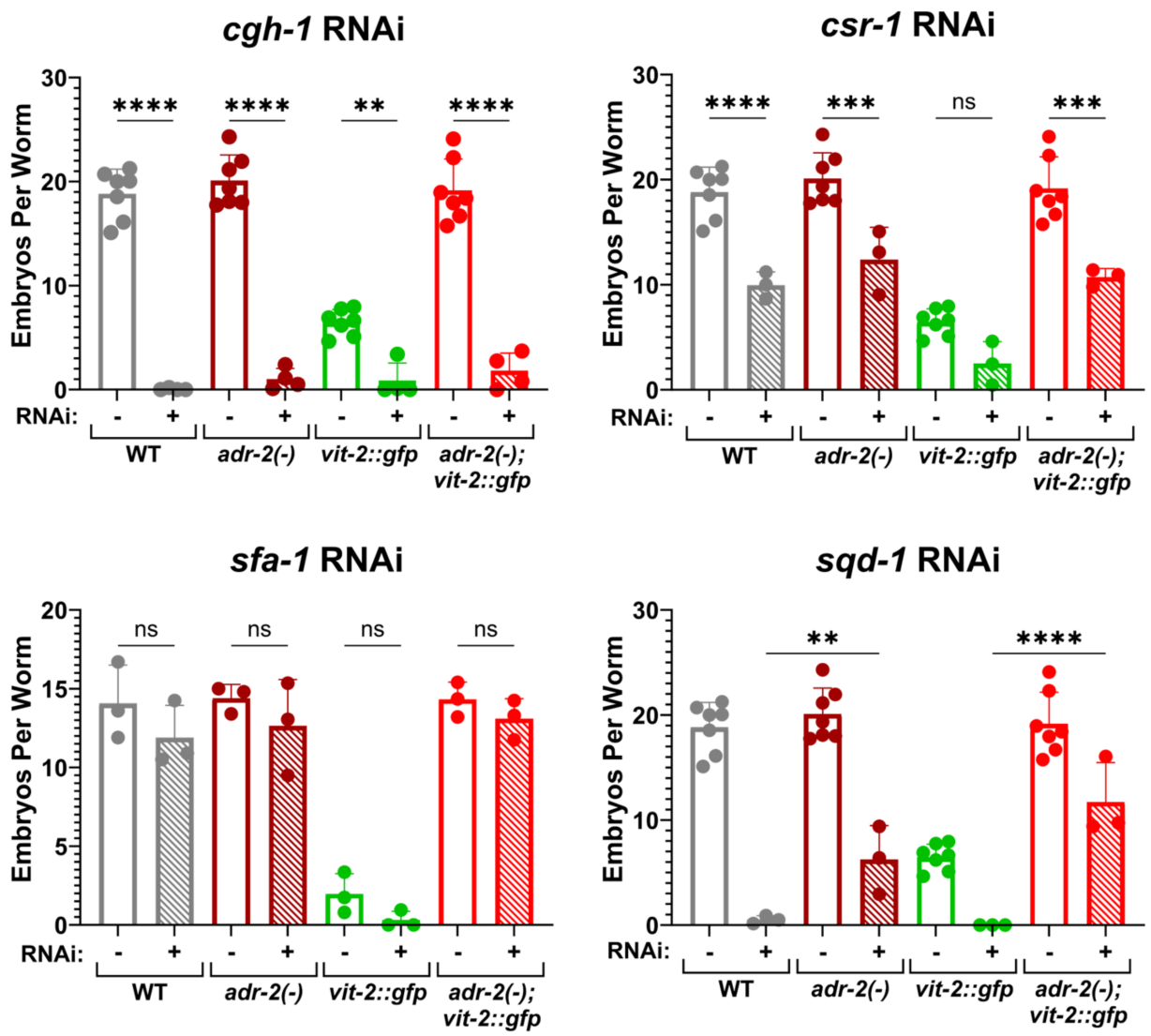
cgh-1 RNAi
csr-1 RNAi
sfa-1 RNAi
sqd-1 RNAi
Embryos Per Worm
RNAi:
-
+
WT
adr-2(-)
vit-2::gfp
adr-2(-); vit-2::gfp
****
**
***
ns

B.

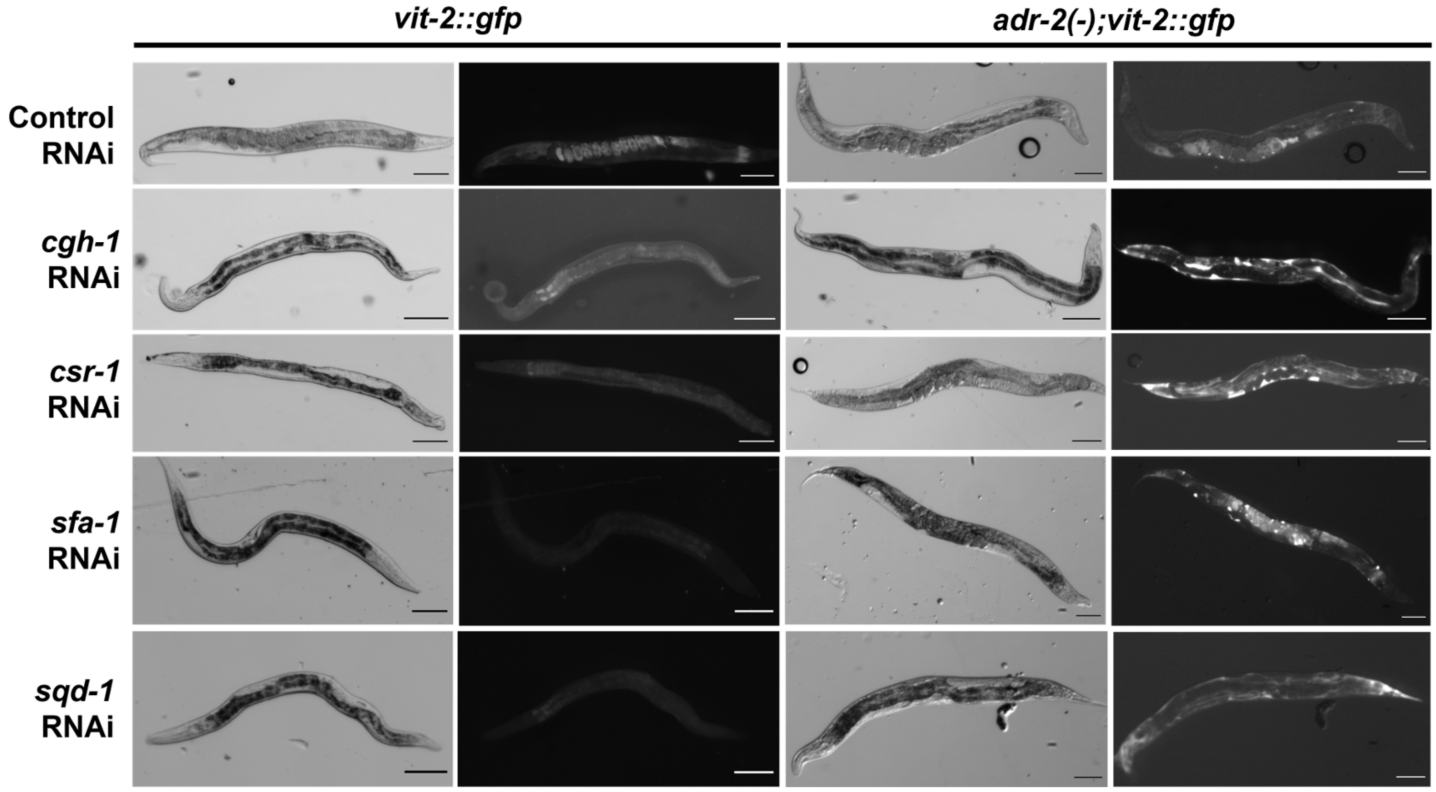
vit-2::gfp
adr-2(-);vit-2::gfp
Control RNAi
cgh-1 RNAi
csr-1 RNAi
sfa-1 RNAi
sqd-1 RNAi

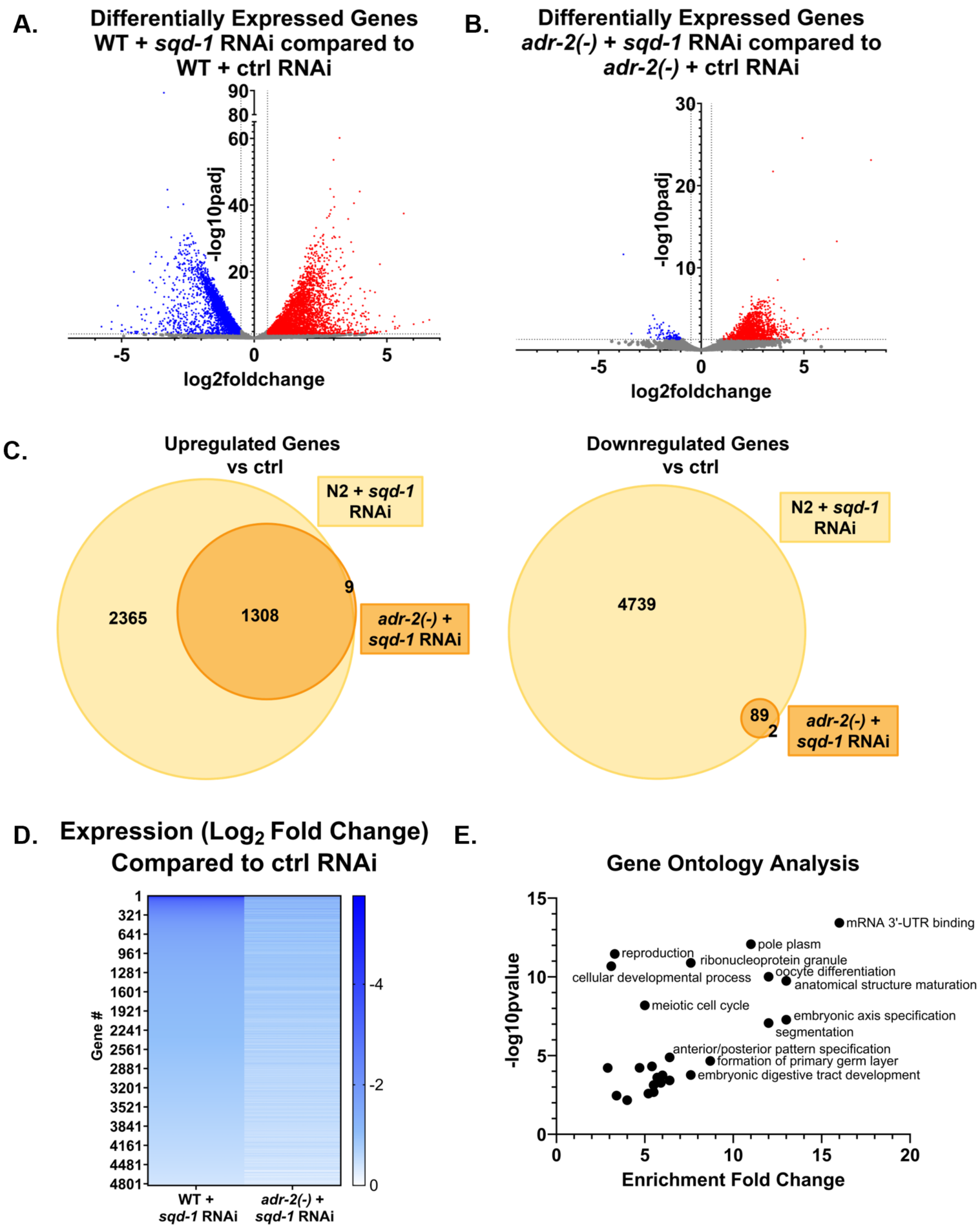
A.
Differentially Expressed Genes
WT + sqd-1 RNAi compared to
WT + ctrl RNAi
-log10padj
log2foldchange
B.
Differentially Expressed Genes
adr-2(-) + sqd-1 RNAi compared to
adr-2(-) + ctrl RNAi
-log10padj
log2foldchange
C.
Upregulated Genes
vs ctrl
N2 + sqd-1 RNAi
adr-2(-) + sqd-1 RNAi
2365
1308
9
Downregulated Genes
vs ctrl
N2 + sqd-1 RNAi
adr-2(-) + sqd-1 RNAi
4739
89
2
D.
Expression (Log2 Fold Change)
Compared to ctrl RNAi
Gene #
WT + sqd-1 RNAi
adr-2(-) + sqd-1 RNAi
E.
Gene Ontology Analysis
-log10pvalue
Enrichment Fold Change
mRNA 3'-UTR binding
pole plasm
reproduction
ribonucleoprotein granule
cellular developmental process
oocyte differentiation
anatomical structure maturation
meiotic cell cycle
embryonic axis specification
segmentation
anterior/posterior pattern specification
formation of primary germ layer
embryonic digestive tract development

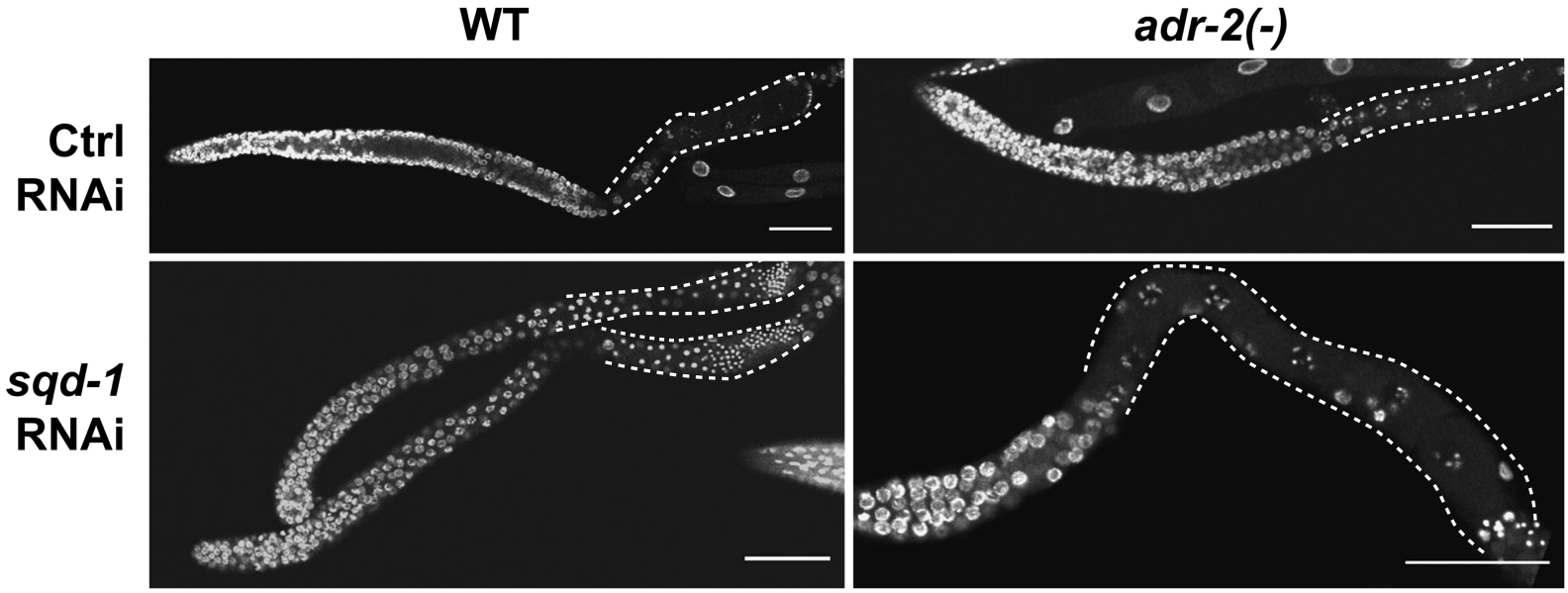
WT
adr-2(-)
Ctrl RNAi
sqd-1 RNAi